이학석사학위논문

A CCN activation parameterization and its impacts on cloud and precipitation simulations

구름응결핵 활성화과정의 모수화 및 구름과 강수 모의에 미치는 영향

2015년 7월

서울대학교 대학원

지구환경과학부

김 민 유

A CCN activation parameterization and its impacts on cloud and precipitation simulations

구름응결핵 활성화과정 모수화 및
구름과 강수 모의에 미치는 영향

지도교수 백 종 진

이 논문을 김민유 이학석사 학위논문으로 제출함
2015년 6월

서울대학교 대학원
지구환경과학부
김 민 유

김민유의 이학석사 학위논문을 인준함
2015년 7월

위 원 장 임 규 호 (인)

부위원장 백 종 진 (인)

위 원 박 죽 진 (인)

Abstract

A parameterization of cloud condensation nuclei (CCN) activation in a rising adiabatic air parcel is developed to link the activation rate to the temperature, vertical velocity, number concentrations of aerosols and cloud droplets, and radius of cloud droplets. The new parameterization considers the activation inside the cloud more precisely, by including the effects of pre-existing cloud droplets on the maximum supersaturation of the air parcel. There is also a modification in the size distribution of aerosols by adding the number of CCN in cloud droplets to the potential aerosol number. The new parameterization is implemented in Thompson aerosol-aware microphysics scheme in Weather Research and Forecasting (WRF) model. An increase in the potential aerosol number leads to an increment in the cloud droplet number and consideration of the pre-existing cloud droplets on supersaturation results in the suppression of the activation process inside the cloud compared with the cloud edge. As a result, the cloud droplet number concentration is the highest in the entrance region of the cloud with the new parameterization, while the activation primarily occurs in the region of high vertical velocity with the previous parameterization. The new parameterization appears to decrease the cloud droplet number in the updraft-limited regime of CCN activation because the suppression of activation due to pre-existing cloud droplets through supersaturation is more significant than

the increase in potential aerosol number. In the aerosol-limited regime, where the aerosol change is more important in activation, the new parameterization increases the cloud droplet number. In the idealized shallow cloud simulations (updraft-limited regime), a decrease in the cloud droplet number increases the cloud droplet radius, thus enhancing the rain formation. In the idealized deep cloud simulations (aerosol-limited regime), an increase in the cloud droplet number reduces the rain formation in the developing stage and an increase in the cloud droplet freezing enhances the latent heating, augmenting the vertical velocity in the mature stage. A precipitation event in the Korean Peninsula on 24 July 2014 is also simulated with climatological aerosol data. The system has both warm clouds and deep clouds with intense precipitation. The new parameterization induces a decrease in the cloud droplet number concentration, increasing the raindrop formation in the shallow cloud and decreasing the ice hydrometeor formation and the convective precipitation, as in the idealized simulations.

Key Words: Activation, nucleation, parameterization, cloud condensation nuclei, cloud droplet number, two-moment bulk microphysics

Student's number: 2013-22968

Contents

List of Figures

1. Introduction

It is well known that aerosols play a significant role in the cloud system as cloud condensation nuclei (CCN) or ice nuclei. The first aerosol indirect effect describes that an increase in the aerosol number concentration generally decreases the droplet radius, thereby increasing cloud albedo (Twomey 1974). A reduction in cloud droplet size also delays and reduces the rain formation and precipitation amount, known as the second aerosol indirect effect (Albrecht 1989). Because the impacts of aerosols on cloud are largely affected by cloud types and environmental conditions, aerosol-cloud interactions in various cloud systems have received considerable attention (e.g., Khain et al. 2009; Lebo and Morrison 2014; Thompson and Eidhammer 2014).

To fully understand the aerosol-cloud-precipitation interactions, efforts are made to consider the effects of the cloud system on aerosols, as well as the effects of aerosols on the cloud system. Nucleation, regeneration and aerosol scavenging are important processes in the interactions between clouds and aerosols (Flossmann et al. 1985). Aerosol processing can be included in the cloud-resolving model by using the two-dimensional bin microphysics model (e.g., Lebo and Seinfeld 2011), by coupling a chemistry model and a weather model (e.g., Grell et al. 2005), or simply by adding the aerosol number or mass concentration as an independent variable in the microphysics scheme (Lim and Hong 2009; Thompson and Eidhammer 2014; Lebo and Morrison

2013). Consideration of aerosol processing allows for a sophisticated estimate of the aerosol number near and inside the cloud system.

Nucleation is the formation of cloud droplets from aerosols and supersaturated vapor and the process which allows aerosols to affect the cloud system. The number of cloud droplets is increased mainly by the nucleation process which is also written as activation process in the microphysics scheme. There are various methods to estimate the activated cloud droplet number in the cloud system. For models that calculate the supersaturation prognostically (e.g., Khain et al. 2009; Lebo and Seinfeld 2011), activation occurs when the ambient supersaturation is greater than the aerosol critical supersaturation. However, supersaturation is not a prognostic variable in most bulk microphysics schemes, thus other methods are required to estimate the activated cloud droplet number. Twomey (1977) formulated the activated cloud droplet number as a function of the temperature, vertical velocity, and number of aerosols using Twomey's lower bound. Abdul-Razzak et al. (1998) improved Twomey's method with a log-normal aerosol size distribution and Abdul-Razzak et al. (2002) used a sectional aerosol representation to formulate the same process with various aerosol distributions. Nenes et al. (2001) introduced the concept of kinematic limitations which interfere with the growth of certain aerosols even with the ambient supersaturation above their critical supersaturations. Nenes and Seinfeld (2003) used the partitioning critical supersaturation, a criterion for dividing the freely growing droplets

and slowly growing droplets, to treat the kinematic limitations. The parameterization was improved to use a lognormal aerosol representation and size-dependent mass transfer coefficient (Fountoukis and Nenes 2005). Further studies were performed to include the giant CCN (Barahona et al. 2010) and the inertially limited CCN (Morales and Nenes 2014) in the scope of activation parameterization. Ming et al. (2006) attempted to address the kinematic limitations using empirical formulations. All of the activation parameterizations described above assume an adiabatic parcel rising in a constant updraft velocity and no cloud droplets at the moment of activation (Ghan et al., 2011). This assumption restricts the parameterizations to be valid only near the base of existing clouds or in the clear air.

In this study, a new activation parameterization is developed for the case where pre-existing cloud droplets are present in an air parcel, to consider in-cloud activation properly. Using the two-moment bulk microphysics scheme with prognostic aerosol number concentration, the new parameterization splits potential aerosols (aerosols that have the potential to act as CCN) into CCN in cloud droplets and aerosols. Next, the activation rate inside the cloud is calculated, considering the growth rate of the pre-existing cloud droplets and the newly activated droplets independently. Detailed formulation is described in section 2. In section 3, the new parameterization is tested in two idealized cloud simulations and a real case simulation. Finally, the summary and conclusions are presented in section 4.

2. Activation parameterization

The parameterizations of activation introduced in the previous section (Abdul-Razzak et al., 1998; Abdul-Razzak et al., 2002; Nenes and Seinfeld, 2003; Ming et al., 2006) follows the same basic strategies to calculate the activated cloud droplet number: the Köhler equation and the saturation adjustment assumption. The following section shows how these approaches parameterize the activation process to calculate the cloud droplet number without a prognostic supersaturation value.

2.1. Previous parameterization

Condensational growth of water droplets is expressed by the following diffusion equation:

$$\frac{dr}{dt} = \frac{G}{r}\left(S - A\frac{1}{r} + B\frac{r_d^3}{r^3 - r_d^3} \right), \tag{1}$$

$$A \equiv 4\sigma M_w / \rho_w RT, \tag{2}$$

where the physical parameters include the radius of water droplet r, the growth coefficient G, the radius of CCN r_d, a constant related to the chemical

properties of CCN B, the surface tension of water σ, the molecular weight of water M_w, the density of liquid water ρ_w, the gas constant of water vapor R, and the temperature T. The critical supersaturation S_c for the CCN of radius r_d is obtained by applying $dr/dt=0$ and $dS/dr=0$ to equation (1):

$$S_c \approx \left(\frac{A^3}{54B} \cdot \frac{1}{r_d^3} \right)^{1/2}. \tag{3}$$

If the ambient supersaturation is greater than the critical supersaturation S_c, then the aerosols of radius r_d activate into cloud droplets.

While condensation occurs in the updraft motion, the change of the ambient supersaturation in a closed adiabatic air parcel is formulated as (Pruppacher and Klett, 1997):

$$\frac{dS}{dt} = \alpha w - \gamma \frac{dq}{dt}, \tag{4}$$

$$\alpha \equiv \frac{gM_w L}{c_p RT^2} - \frac{gM_a}{RT}, \tag{5}$$

$$\gamma \equiv \frac{pM_a}{e_s M_w} + \frac{M_w L^2}{c_p RT^2}, \tag{6}$$

where S is the ambient supersaturation, w is the vertical velocity of the air parcel, q is the mixing ratio of vapor condensed into liquid phase, g is the

gravitational acceleration, M_a is the molecular weight of dry air, L is the latent heat of vaporization of water, c_p is the isobaric heat capacity of dry air, p is the ambient pressure, and e_s is the saturation pressure of water vapor.

The saturation adjustment method assumes that the microphysics scheme has a longer time step than the time scale of droplet growth by nucleation and condensation. Ambient supersaturation is adjusted to 0 at the end of each time step, and the nucleation process occurs only when the ambient supersaturation is increasing. Thus, the cloud droplet number is determined by the maximum supersaturation of the air parcel $S_{\max}$ within a time step. At the maximum supersaturation (dS/dt = 0 in equation (4)), the increase of the ambient supersaturation by adiabatic cooling is balanced with the decrease of the ambient supersaturation by the vapor depletion through diffusion process:

$$\alpha w = \gamma \frac{dq}{dt}. \tag{7}$$

The depleting rate of water vapor dq/dt is the same as the growth rate of the water droplets by nucleation and condensation. Assuming that the air parcel does not contain any pre-existing cloud droplets and all cloud droplets are grown from aerosols ($dq/dt = (dq/dt)_{\mathrm{wfa}}$), the growth rate of cloud droplets at the maximum supersaturation is:

$$\left(\frac{dq}{dt}\right)_{\text{wfa}} = \frac{4\pi\rho_w}{\rho_a}\left(\int_0^{S_{\max}} r^2 \frac{dr}{dt}\frac{dN_{\text{wfa}}}{dS_c} dS_c\right), \tag{8}$$

where N_{wfa} is the number concentration of aerosols and ρ_a is the density of the ambient air.

Assuming that curvature and solute effects are negligible beyond the point of activation, equation (1) is reduced to:

$$\frac{dr}{dt} = \frac{G}{r}S, \tag{9}$$

and its time integration is:

$$r^2(t_{\max}) = r^2(t_{\text{act}}) + 2G\int_{t_{\text{act}}}^{t_{\max}} S dt, \tag{10}$$

where t_{act} is the time of the activation and $t_{\max}$ is the time of the maximum supersaturation. The first term in the right hand side refers to the droplet size at the time of activation, and the second term signifies the size increment from activation until the maximum supersaturation is reached. By applying equations (9) and (10) into equation (8), at the maximum supersaturation, the growth rate of the cloud droplets activated from aerosols is expressed as:

$$\left(\frac{dq}{dt}\right)_{\text{wfa}} = \frac{4\pi\rho_w}{\rho_a} G S_{\max} \int_0^{S_{\max}} \left(r^2(t_{\text{act}}) + 2G \int_{t_{\text{act}}}^{t_{\max}} S dt \right) \frac{dN_{\text{wfa}}}{dS_c} dS_c. \qquad (11)$$

The first term inside the integration part is dominant when the ambient supersaturation is similar to the critical supersaturation of aerosols, and the second term is dominant when the ambient supersaturation is larger than the critical supersaturation. Using these characteristics, Nenes and Seinfeld (2003) defined the partitioning critical supersaturation S_{part} where the two terms are similar in magnitude, and then calculated the integration part by considering only the first term for aerosols with larger critical supersaturation than S_{part} and only the second term for the others.

Bringing equation (11) into equation (7) results in:

$$\alpha w = \frac{4\pi\gamma\rho_w}{\rho_a} G S_{\max} \int_0^{S_{\max}} \left(r^2(t_{\text{act}}) + 2G \int_{t_{\text{act}}}^{t_{\max}} S dt \right)^{1/2} \frac{dN_{\text{wfa}}}{dS_c} dS_c, \qquad (12)$$

where S_{max} is calculated from the temperature, vertical velocity and aerosol number concentration.

The maximum cloud droplet number concentration ($N_{c,\max}$) that can exist in an air parcel can be written as:

$$N_{c,\max} = \int_0^{S_{\max}} \frac{dN_{\text{wfa}}}{dS_c} dS_c. \qquad (13)$$

If the pre-existing cloud droplet number is smaller than the calculated maximum cloud droplet number, then the model supposes that activation occurs in the air parcel and takes the latter value as the cloud droplet number.

In the bulk microphysics models, when the aerosol number is calculated prognostically, the activation scheme removes an aerosol particle to form a new cloud droplet. In each of the grid points, the model calculates the maximum cloud droplet number from the aerosol and environmental properties of each of the gird points. For these simplified model, there are two approaches to estimate the potential aerosol number concentration. The first approach is to ignore the cloud droplets in the grid point to estimate potential aerosols (Thompson and Eidhammer 2014). The second approach is to include the CCN in the pre-existing cloud droplets to the potential aerosols (Morrison and Gettleman 2008), which must have a larger number of the potential aerosols than the first approach. In this study, two types of consideration on the potential aerosols are also compared.

2.2. New parameterization

The main improvement of the new parameterization from the previous parameterization shown above is that the diffusion (condensation) process on the pre-existing cloud droplets is also considered in calculating the maximum supersaturation. Except for the cloud base, the nucleation process occurs in the environment where cloud droplets and aerosols coexist. In the updraft motion, the supersaturated vapor is diffused onto not only aerosols (through nucleation process) but also cloud droplets (through droplet growth process). Because larger droplets grow fast and preferentially, the diffusion process occurs on aerosols (nucleation occurs) only if the increasing rate of supersaturation exceeds the growth rate of pre-existing cloud droplets. Thus, in a strict sense, the assumption made in the previous section must be modified to consider the pre-existing cloud droplets together with the aerosols. In this study, the growth of the droplets newly activated from the aerosols and the growth of the pre-existing droplets are considered simultaneously to include the effects of the pre-existing cloud droplets on the activation process via supersaturation adjustment.

To consider both aerosols and cloud droplets, the potential aerosols must be divided into the already activated one (CCN in cloud droplets) and inactivated one (aerosols). A log-normal size distribution is assumed for the potential aerosols:

$$\frac{dN_{\mathrm{CCN}}}{d\ln r_d} = \frac{N_{\mathrm{CCN,Po}}}{\sqrt{2\pi}\ln\sigma}\exp\left[-\frac{\ln^2\left(r_d/r_g\right)}{2\ln^2\sigma}\right], \tag{14}$$

where σ is the geometric standard deviation, and r_g is the geometric mean radius. In this case, the potential aerosol number concentration ($N_{\mathrm{CCN,Po}}$) is the sum of the aerosol number concentration (N_{wfa}) and the cloud droplet number concentration (N_c). Since nucleation preferentially occurs on large aerosols, the relationship between the cloud droplet number and the smallest radius of activated CCN (r_{cut}) can be obtained (Lebo and Morisson 2013):

$$r_{\mathrm{cut}} = r_g \exp\left[\sqrt{2}\ln\sigma \mathrm{erf}^{-1}\left(1-2N_c/N_{\mathrm{CCN,Po}}\right)\right]. \tag{15}$$

Here, erf(x) is the error function. All of the unactivated aerosols have smaller radius than r_{cut}.

If growth of dry aerosols and cloud droplets are considered simultaneously, then the growth rate of droplets dq/dt can be expressed as:

$$\frac{dq}{dt} = \left(\frac{dq}{dt}\right)_{\mathrm{wfa}} + \left(\frac{dq}{dt}\right)_c. \tag{16}$$

The first term on the right hand side is the growth rate of newly activated droplets, which is the same as equation (8). The second term is the growth

rate of pre-existing cloud droplets, which is formulated as:

$$\left(\frac{dq}{dt}\right)_c = \frac{4\pi\rho_w}{\rho_a}\left(r^2(t_{\max})\frac{dr_c}{dt}N_c\right). \tag{17}$$

Because the cloud droplet number does not change during the droplet growth process, equation (17) is simpler than equation (8). For cloud droplets that are already activated ($t_{act} = t_0$), equation (10) is rewritten as:

$$r^2(t_{\max}) = r_c^2 + 2G\int_{t_0}^{t_{\max}} S dt, \tag{18}$$

where r_c is the initial radius of cloud droplets. For pre-existing cloud droplets, the initial size is much larger than the size increment from t_0 to t_{max}, thus equation (18) can be reduced to:

$$r^2(t_{\max}) \approx r_c^2. \tag{19}$$

By combining equations (9), (17), and (19), the growth rate of pre-existing cloud droplets is:

$$\left(\frac{dq}{dt}\right)_c = \frac{4\pi\rho_w}{\rho_a} G S_{\max} r_c N_c. \tag{20}$$

By substituting equations (11), (16), and (20) into equation (7), the following equation is obtained:

$$\alpha w = \frac{4\pi\gamma\rho_w}{\rho_a} G S_{\max} \left[r_c N_c + \int_0^{S_{\max}} \left(r^2(t_{\text{act}}) + 2G \int_{t_{\text{act}}}^{t_{\max}} S dt \right)^{1/2} \frac{dN_{\text{CCN}}}{dS_c} dS_c \right]. \qquad (21)$$

Using the integration method from Nenes and Seinfeld (2003) with sectional representation of the CCN, equation (21) can be rewritten as:

$$\frac{4\pi\gamma\rho_w}{\alpha w \rho_a} G S_{\max} \left[\left(\frac{G}{\alpha w} \right)^{1/2} \sum_{j=i_{\text{cut}}}^{i_{\text{part}}} \frac{N_j}{S_c^j - S_c^{j-1}} \cdot \left[\frac{x}{2} (S_{\max}^2 - x^2)^{1/2} + \frac{S_{\max}^2}{2} \arcsin \frac{x}{S_{\max}} \right]_{x=S_c^{j-1}}^{x=S_c^j} \right.$$

$$\left. + \frac{1}{3} A \left[\left(\frac{N_{i_{\max}}}{S_c^{i_{\max}} - S_c^{i_{\max}-1}} \right) \ln \frac{S_{\max}}{S_c^{i_{\max}-1}} + \sum_{j=i_{\text{part}}}^{i_{\max}-1} \left(\frac{N_j}{S_c^j - S_c^{j-1}} \right) \ln \frac{S_c^j}{S_c^{j-1}} \right] + r_c N_c \right] - 1 = 0, \qquad (22)$$

$$\frac{4A^2}{9S_{\text{part}}^2} = \frac{G}{\alpha w} (S_{\max}^2 - S_{\text{part}}^2), \qquad (23)$$

where N_j is the number of CCN in the j$^{\text{th}}$ bin and S_c^j is the critical supersaturation of CCN in the j$^{\text{th}}$ bin. The subscript 'part' refers to the bin with critical supersaturation of S_{part}, the subscript 'max' refers to the bin with critical supersaturation of $S_{\max}$, and the subscript 'cut' refers to the bin with radius r_{cut}. The increment of the cloud droplet number by the activation

process is the number of aerosols that are not activated in prior processes but have critical supersaturation less than S_{max}:

$$\Delta N_c = \int_{S_{cut}}^{S_{max}} \frac{dN_{CCN}}{dS_c} dS_c. \quad (24)$$

In this case, the calculated number of activated CCN does not compromise the pre-existing cloud droplet number.

The procedure to calculate the increment of the cloud droplet number by the activation process is shown in the flow chart (Fig. 1). From the dynamics of the model, the temperature, the vertical velocity, the number concentrations of the aerosols and cloud droplets, and the radius of cloud droplets are given. With the prescribed standard deviation and geometric mean radius, the activation scheme determines the maximum radius of aerosols r_{cut} and its critical supersaturation S_{cut}.

The first estimation of S_{max} is given as the maximum supersaturation attained when the activation does not occur (only the condensation occurs), which is the largest value of possible maximum supersaturations. Because the activation occurs only if the ambient supersaturation is greater than S_{cut}, the activated droplet number is calculated only if the first estimation of S_{max} is greater than S_{cut}. Otherwise the cloud droplet number does not change due to the activation process.

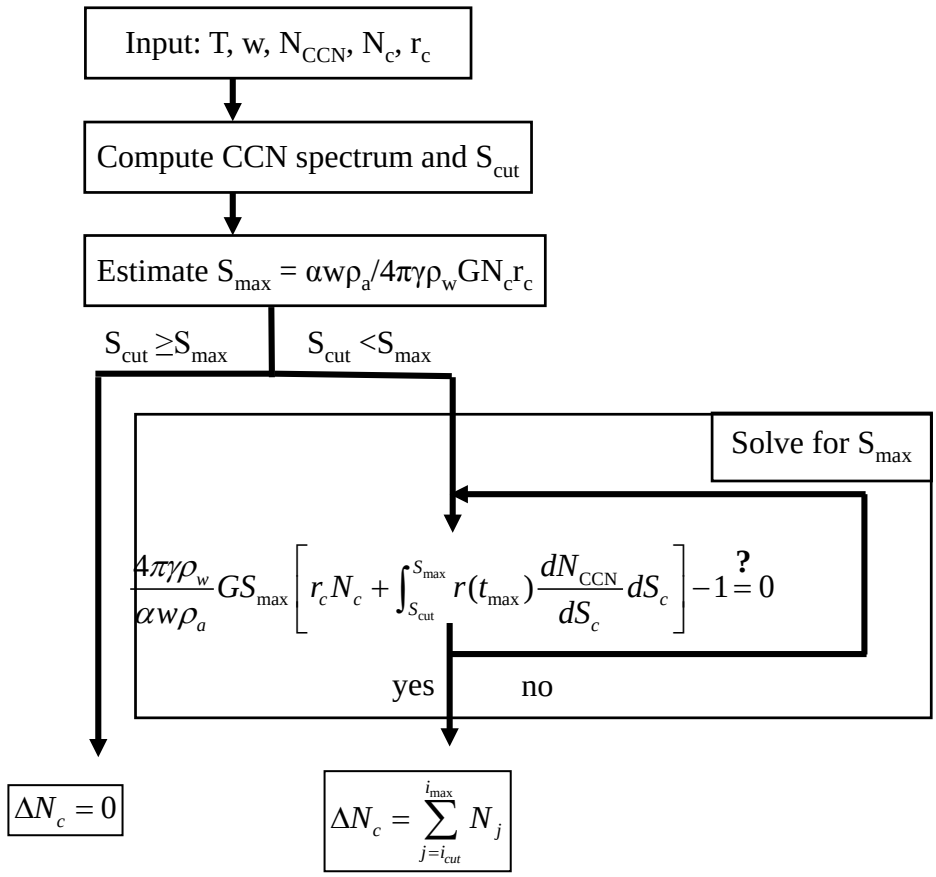

Figure 1. Flow chart for the new parameterization of activation.

If the activation occurs, equations (22) and (23) are used to find the maximum supersaturation S_{max} through iterations. Using the final value of S_{max}, the activated cloud droplet number is calculated by equation (24).

By including the effect of pre-existing cloud droplets on supersaturation, the activation parameterization can demonstrate the extent that pre-existing cloud droplets influence the activation inside the cloud. By specifying the vertical velocity and the potential aerosol number concentration with r_g = 0.08 μm and σ_g = 1.8, the cloud droplet number concentration (CDNC) varies with the number and size of pre-existing cloud droplets (Figs. 2 and 3). To distinguish the pre-existing cloud droplets from the resultant cloud droplets after activation, the term 'initial cloud droplet fraction' is introduced as the ratio of the pre-existing cloud droplet number to the potential aerosol number, and the term 'activation fraction' denotes the ratio of the resultant cloud droplet number to the potential aerosol number. It is shown that the activation fraction with pre-existing cloud droplets (with the initial cloud droplet fraction larger than 0 in Fig. 1) is smaller than the cases with no droplet (with the initial cloud droplet fraction of 0), except the cases when the initial cloud droplet fraction is higher than the activation fraction with no droplet (Fig. 2). The increase in the initial cloud droplet fraction causes a decrease in the activation fraction, as a result of the increased number of fast growing droplets. The decreasing trend continues until the activation fraction reaches the initial cloud droplet fraction, indicating that, with a sufficient number of

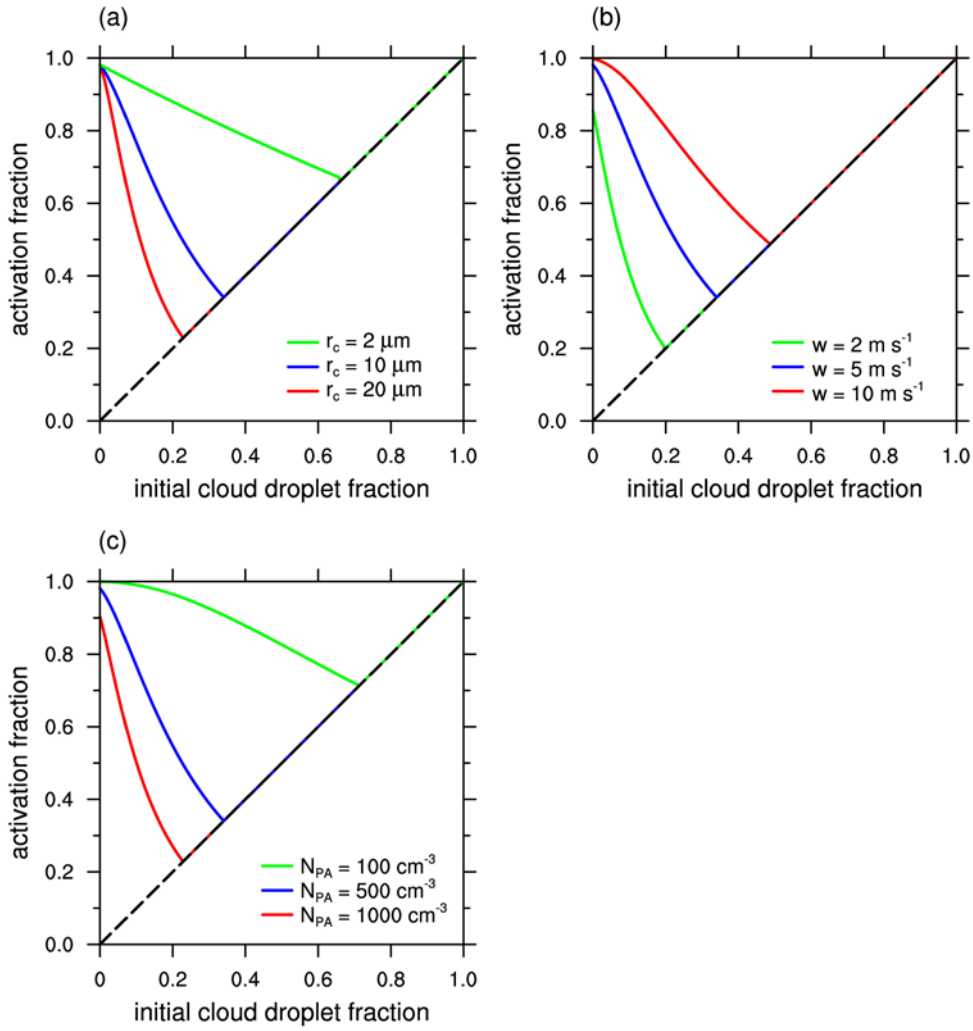

Figure 2. Activation fraction–initial cloud droplet fraction profiles with (a) various droplet radii (2 µm for green, 10 µm for blue, and 20 µm for red lines), (b) various vertical velocities (2 m s^{-1} for green, 5 m s^{-1} for blue, and 10 m s^{-1} for red lines), and (c) various potential aerosol number concentrations (100 cm^{-3} for green, 500 cm^{-3} for blue, and 1000 cm^{-3} for red lines). Dashed lines denote the case without activation process.

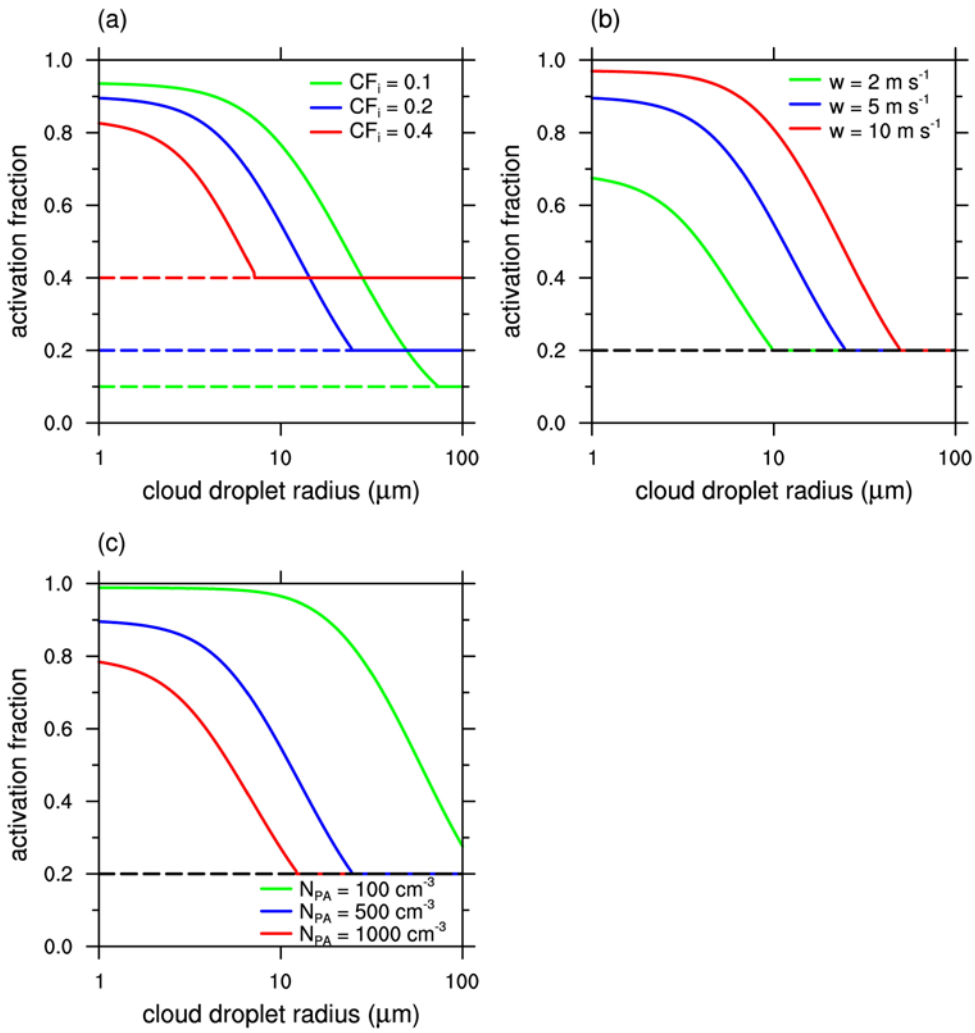

Figure 3. As in Fig. 2, but for activation fraction–cloud droplet radius profiles with (a) various initial cloud droplet fractions (0.1 for green, 0.2 for blue, and 0.4 for red lines), (b) various vertical velocities, and (c) various potential aerosol number concentrations.

pre-existing cloud droplets, the activation process does not occur and the supersaturated vapor is depleted only by the droplet growth process.

The decrease in activation fraction with increasing initial cloud droplet fraction accelerates with larger droplets (Fig. 2a). For small values of the droplet radius, the pre-existing cloud droplets do not substantially influence the activation fraction, because their growth rate is not much faster than the newly activated droplets. However, as the droplets become larger, the effect of the pre-existing cloud droplets on supersaturation becomes larger to suppress or even stop the activation in a rising parcel. Similarly, if the initial cloud droplet fraction is high, then the activation fraction decreases with smaller droplets in a larger amount, suggesting increased effects of pre-existing cloud droplets (Fig. 3a). As could be predicted from equation (21), the pre-existing cloud droplets reduce the CDNC as well as the maximum supersaturation and the suppression effect increases when there are a large number of large droplets.

For the environments without cloud droplets, it is well known that the vertical velocity and the aerosol number concentration are the most important factors in the determination of activation fraction (Reutter et al. 2009). As the vertical velocity increases, the activation fraction increases (Figs. 2b and 3b). For a low vertical velocity, the reduction of the activation fraction occurs with a low initial cloud droplet fraction and small droplet radii, indicating that the suppression effect is more significant with a slower supply of excess vapor.

On the other hand, an increase in the potential aerosol number concentration leads to a decrease in the activation fraction and intensifies the suppression of the activation due to pre-existing cloud droplets (Figs. 2c and 3c). It can also be deduced that the pre-existing cloud droplets largely influence the activation process when the supersaturated vapor is not sufficient to activate a large portion of the aerosols. In summary, the suppression of activation is significant with large cloud droplets and high initial cloud droplet fraction under less supersaturated conditions such as low vertical velocity and high aerosol number.

The new parameterization described above is expected to reduce the cloud droplet number concentration by accounting for the competition between aerosols and cloud droplets for supersaturated vapor. In this study, the new parameterization is implemented in a numerical model and the effects of pre-existing cloud droplets on the activation is investigated in the idealized cloud simulations and a real precipitation case simulation.

3. Results and discussion

3.1. Idealized cloud simulations

3.1.1. Experimental setup

To implement the new activation parametrization, this study uses Weather Research and Forecast (WRF) model version 3.6 developed by the National Center for Atmospheric Research (NCAR). MYJ planetary boundary layer scheme (Janjic 1994) is used only for the warm cloud simulation and no other parameterizations except the microphysics scheme are used. As a microphysics scheme, Thompson aerosol-aware scheme (Thompson and Eidhammer 2014) is used. Both the mixing ratio and the number concentration of cloud droplets, raindrops and ice crystals, the mixing ratio of snow and graupel, and the number concentration of water-friendly aerosols and ice-friendly aerosols are calculated prognostically. For aerosol processing, nucleation, regeneration, scavenging, emission from the surface, and advection are considered. For activation parameterization, a lookup table created by Feingold and Heymsfield (1992) with additional changes by Eidhammer et al. (2009) is used. The table determines the activation fraction from the vertical velocity, aerosol number concentration, temperature, and

prescribed aerosol properties. For in-cloud activation, the presence of cloud droplets is ignored in the parameterization as there is no cloud droplet at all. There is no adjustment in the aerosol size distribution (number of potential aerosol) and supersaturation due to pre-existing cloud droplets. The CDNC is updated only if the calculated cloud droplet number is larger than the pre-existing cloud droplet number.

In this study, the new activation parameterization is applied to examine the effects of pre-existing cloud droplets on supersaturation and activation. NEW signifies the case with activation parameterization which considers effects of pre-existing cloud droplets, whereas MG08 cases follow the method presented in Morrison and Gettleman (2008), where pre-existing cloud droplets does not affect supersaturation. In both simulations, the size distribution of aerosols follows equation 14 and assumes the aerosols larger than r_{cut} are CCN in the cloud droplets. Thompson and Eidhammer (2014) also ignores pre-existing cloud droplets as a component of the potential aerosols (by setting $N_{\mathrm{CCN,Po}} = N_{\mathrm{wfa}}$), thus the number of the potential aerosols are smaller in the cloud compared with the MG08 and NEW cases. By including the TE14 cases, the effect of pre-existing cloud droplets on the aerosol size distribution could be compared with the effect on supersaturation in terms of activation.

To see the differences among the three activation parameterizations, two types of idealized 2-dimensional simulations are performed: a warm

orographic cloud simulation and a deep single-cell cloud simulation. To simulate an orographic cloud, the sounding data from Osan, South Korea at 00 UTC 19 September 2012 is used (Fig. 4a). There was an inversion layer between 2.8 and 3-km height, and light precipitation (less than 10 mm) was observed near Osan. A bell-shaped mountain of 1-km height and 10-km half-width is set at the domain center to trigger convection. The horizontal wind speed is 10 m s^{-1} above the height of 1 km and linearly decreases to zero at the surface. The model grid size is 1 km in the horizontal direction and 22 to 44 m in the vertical direction to encompass the total domain of 200-km width and 5-km height. The time step is 3 s and the model is integrated for 3 h.

To simulate a single-cell cloud, the sounding data from Osan at 06 UTC 10 June 2014 is selected (Fig. 4b). For the upper layer above 400 hPa, the sounding data at 00 UTC 10 June is used. There was a precipitation amount of 70 mm near Osan and the convective available potential energy was 1091 J, enough to develop deep convection. The cloud is triggered by a warm bubble, which has a maximum perturbation of 3 K and a radius of 3 km, with zero background wind. The model grid size is 100 m and the domain size is 20 km in both the horizontal and vertical scales. The time step is 0.5 s. The model is integrated for 60 min, and the single-cell cloud develops at 6 min and dissipates at approximately 50 min.

The potential aerosol size distribution is assumed to have a geometric radius of 0.08 μm and a standard deviation of 1.8. The aerosol number

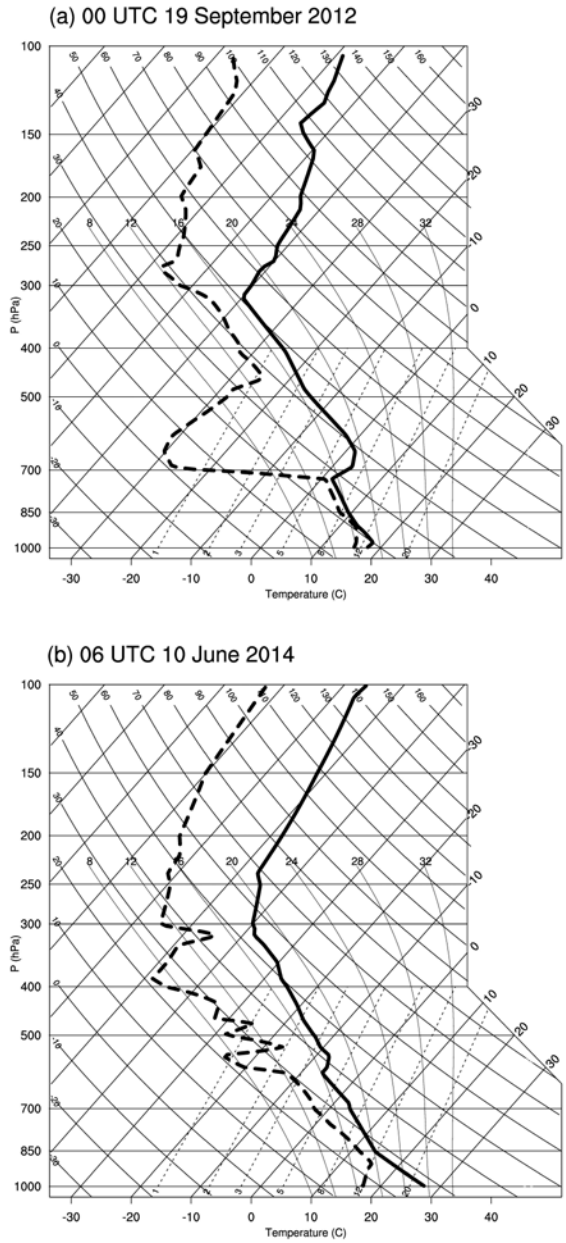

Figure 4. Skew T-log P diagram from Osan, South Korea for the initial sounding of (a) the warm orographic cloud simulation and (b) the deep single-cell cloud simulation.

concentration decreases exponentially as the height increases, from the base aerosol number concentration (BANC) near the surface to one-fourth of the BANC in the free atmosphere. 17 different BANCs are tested, from 60 to 4000 cm^{-3} for the orographic cloud simulations and from 120 to 8000 cm^{-3} for the single-cell cloud simulations. For representative cases, clean, control, and polluted simulations are set using the BANC values of 100, 500, and 2000 cm^{-3} for the orographic cloud cases, respectively, and 200, 1000, and 4000 cm^{-3} for the single-cell cloud cases, respectively.

3.1.2. Warm cloud simulations

In the orographic cloud simulation, a warm cloud of approximately 1 km in height and 20 km in width is formed. The cloud develops at the very start of the simulation (less than 5 min after the simulation starts) and the analysis is primarily performed from 90 to 150 min (1 h) when the cloud is stable in all cases. The cloud is composed mostly of cloud droplets, with a small amount of rain in the downwind side (Fig. 5). The air flow over the mountain induces a weak vertical motion in the upwind side of the mountain. As the air moves, it experiences a gradual increase in vertical velocity having a maximum value of 0.5 m s^{-1} at 5 km ahead of the mountain top. In the upwind region where the vertical velocity increases, activation could occur and the cloud system is affected by the parameterization methods. The raindrop

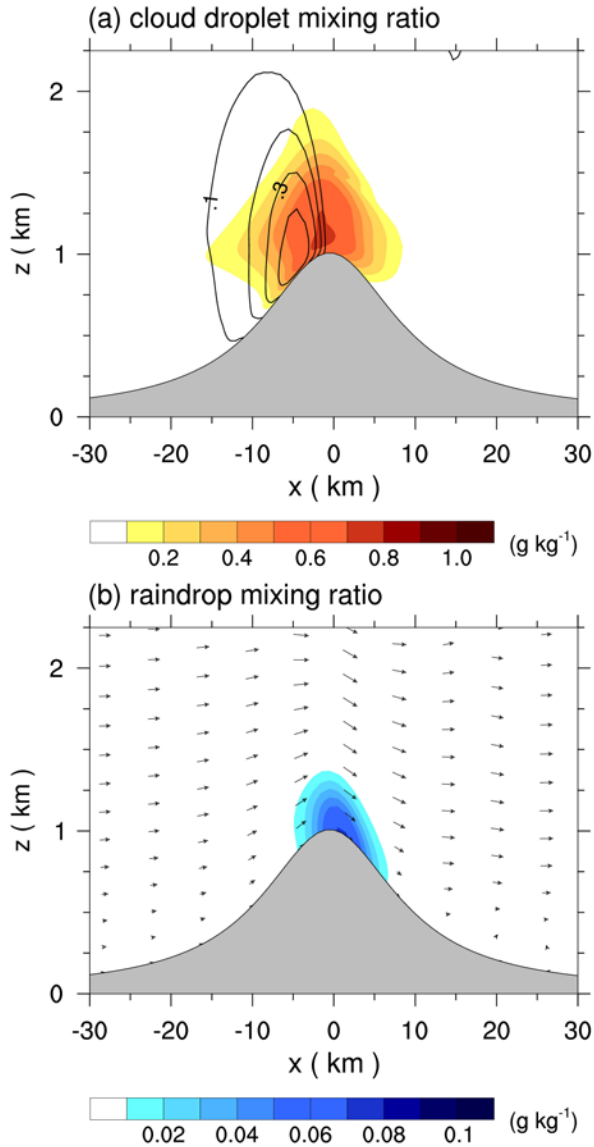

Figure 5. Vertical cross section of 1-hour averaged (a) cloud droplet mixing ratio and (b) raindrop mixing ratio from the NEW case with the BANC of 500 cm^{-3}. Black contour lines in Fig. 5a represent vertical velocities and black arrows in Fig. 5b denote wind vectors.

mixing ratio is quite sensitive to the parameterizations and the BANC, but is always concentrated in the downwind side of the mountain. There is a small amount of rain in the system compared with the cloud droplets (approximately 10% of cloud droplet mixing ratio in the control case). The cloud droplet mixing ratio is nearly constant in the upwind side and changes less than 30% in the downwind side all of the cases.

The CDNC is directly affected by the activation parameterizations and the BANC (Fig. 6). As the BANC increases, the CDNC increases, but the ratio of CDNC to BANC decreases because the activation fraction decreases with increasing potential aerosol number (Figs. 2c and 3c). The clouds develop further downwind as the CDNC increases, suggesting that cloud droplets remain in the clouds longer. Among three parameterizations, the MG08 cases show the highest CDNC and the NEW cases show the lowest CDNC. The MG08 cases show larger CDNC than the TE14 cases because the MG08 parameterization calculates more activation with higher potential aerosol number by including previously activated aerosols in the potential aerosols. In both cases, the highest CDNC appears in the bottom of the cloud center, and the CDNC is smaller at higher altitudes and in the sides of the clouds. The spatial distribution of the CDNC is quite similar to the vertical velocity distribution (Fig. 5a), especially in the polluted cases. It can be suggested that the CDNC is largely influenced by the vertical velocity – high vertical velocity directly corresponds to a large CDNC – in the MG08 and TE14 cases.

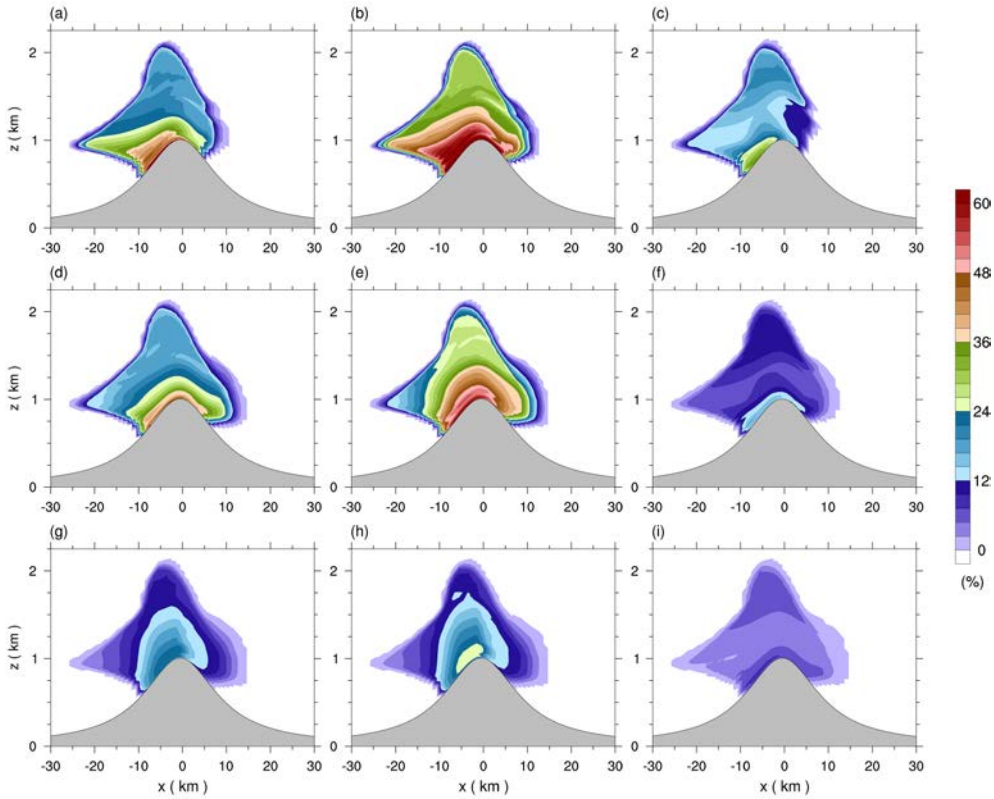

Figure 6. Vertical cross section of 1-h averaged CDNC normalized by BANC. Columns correspond to the activation parameterizations – the TE14 cases for the left, the MG08 cases for the middle, and the NEW cases for the right – and rows correspond to the BANCs – the clean cases for the top, the control cases for the middle, and the polluted cases for the bottom –.

However, the NEW cases show different spatial distribution of the CDNC. These cases all have the maximum CDNC in the bottom of the cloud center, and they also have the second maximum near the top of the clouds. The CDNC is lower in all of the cloud regions than the MG08 and TE14 cases but is prominent in the middle of the clouds. The spatial distribution of the CDNC differs from the other two parameterizations because of the inclusion of pre-existing cloud droplets in the calculation of supersaturation. Pre-existing cloud droplets inhibit in-cloud activation, even with a high vertical velocity, so that the CDNC in the NEW cases depends on the pre-existing droplets as well as the vertical velocity.

Comparing the activation rates in different parameterizations and the BANCs allows for further investigation of the low CDNC in the middle cloud of the NEW cases (Fig. 7). As the BANC increases, the activation rates increase, but the normalized activation rates decrease, as does the CDNC. It is also shown that the activation rates in the middle of the cloud is lower than in the bottom and top regions because the area where activation mostly occurs is farther from the high velocity regions near the mountain top. Activation mostly occurs in the upwind edge of the cloud, where the cloud first develops but in-cloud activation also appears in some cases. In-cloud activation is significant in the polluted cases of the MG08 and TE14, whereas the NEW cases show little or no activation in the same range. The MG08 and TE14 parameterizations ignore the growth of pre-existing cloud droplets, and the

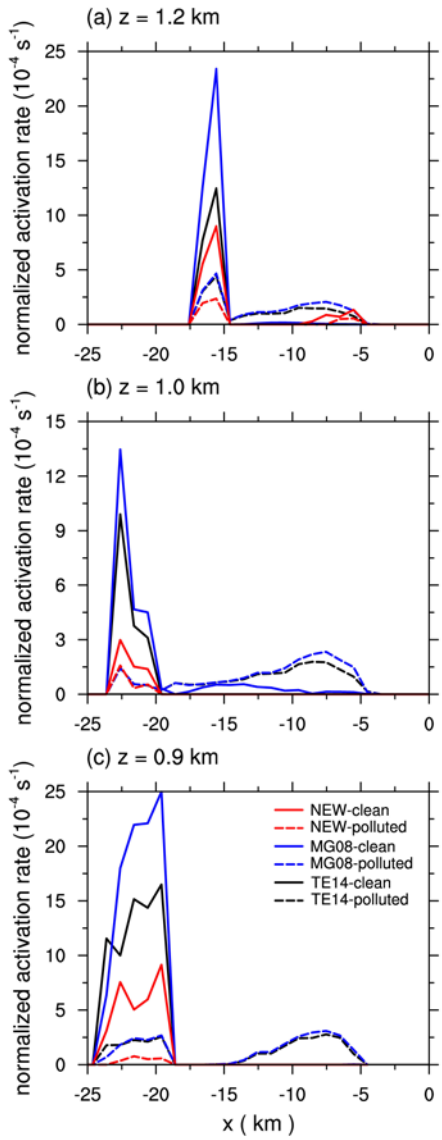

Figure 7. In-cloud and 1-h averaged activation rate normalized by BANC at the height of (a) 1.2 km, (b) 1.0 km, and (c) 0.9 km. Red line signify the NEW cases, blue lines signify the MG08 cases, and black lines signify the TE14 cases. Solid lines are the clean cases and dashed lines are the polluted cases.

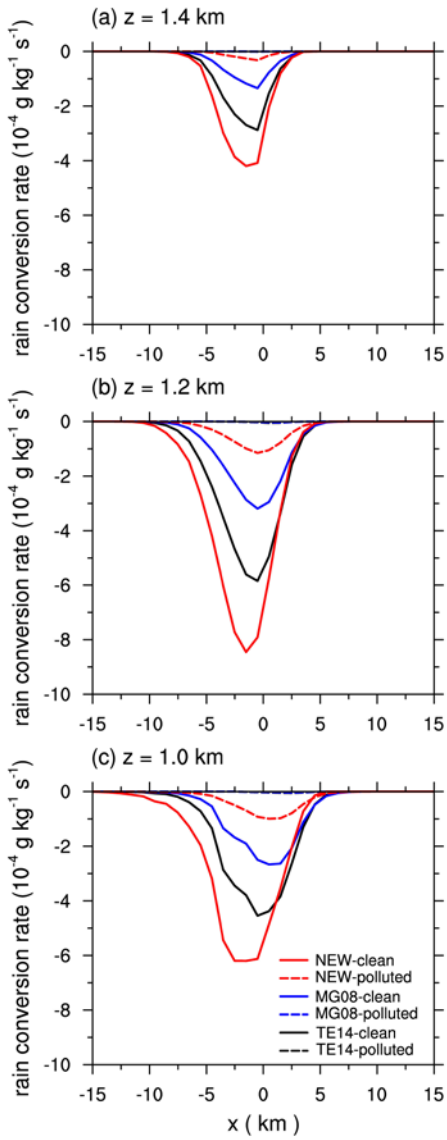

Figure 8. As in Fig. 7, but for the conversion rate of cloud droplets into raindrops at the height of (a) 1.4 km, (b) 1.2 km, and (c) 1.0 km.

CDNC increases as the vertical velocity increases up to the maximum value in the middle of the cloud. However, in the NEW cases (the middle column of Fig. 6), limited activation could occur inside the cloud due to consumption of supersaturation by pre-existing droplets. The activation rate is reduced in the NEW cases also at the cloud edge, but the absence of activation in the middle area suppresses the further increase of the CDNC as the air moves into the cloud center, resulting in a smaller CDNC in the middle of the cloud compared with the values in the top and the bottom.

Because there are small differences in the cloud droplet mixing ratio compared with the huge changes in the CDNC, the cloud droplet radius is small for the cases with large CDNC. A small cloud droplet radius directly affects the autoconversion process so that the conversion of cloud droplets into raindrops occurs earlier in the upwind side in the clean cases (Fig. 8). The NEW cases show the largest amount of raindrop formation among all three parameterizations, which is consistent with the smallest CDNC. The conversion rates show why the cloud develops far downwind side in the polluted cases (the bottom row of Fig. 6). The polluted cases produce a lower amount of raindrops with more cloud droplets remaining in the downwind side compared with the clean cases.

As the BANC increases, the CDNC increases and the cloud droplet fraction decreases (Figs. 9a and 9b). The sensitivity of CDNC to BANC varies among the three activation parameterizations, where the CDNC increases the most in

the TE14 cases as the BANC increases. The cloud droplet fraction trend is the opposite to the trend of the CDNC, with the lowest sensitivity in the TE14 cases. The differences between the TE14 and MG08 cases decrease as the BANC increases, indicating that changes in the potential aerosol number are not important in the cases with a high concentration of aerosols. The NEW cases show the lowest CDNC and cloud droplet fraction and the differences between the MG08 and NEW cases are larger than the differences of the TE14 and MG08 cases. It could be suggested that the effect of pre-existing cloud droplets on supersaturation remains significant, even with a high BANC, and is more important than the increase in potential aerosol number. The cloud droplet mixing ratio does not change much as the BANC changes (Fig. 9c). The cloud droplet content increases less than 1.5 times, whereas the CDNC increases approximately 10 to 20 times as the BANC increases approximately 70 times. The cloud microphysics is therefore affected primarily by the CDNC changes, and the cloud droplet radius decreases as the BANC increases (Fig. 9d), producing less raindrops (Fig. 9e). The decrease in the raindrop mixing ratio directly influences the precipitation rate, which decreases rapidly as the BANC increases (Fig. 9f).

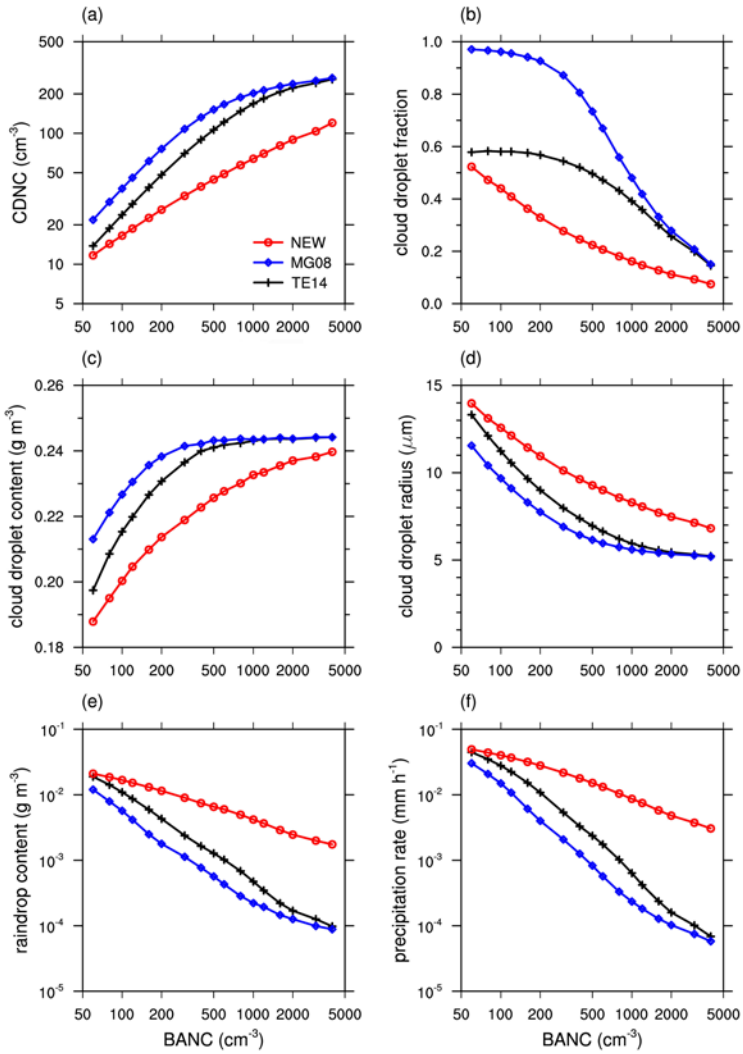

Figure 9. In-cloud and 1-h averaged (a) CDNC and (b) cloud droplet fraction, domain and 1-h averaged (c) cloud droplet mixing ratio, (d) cloud droplet radius, (e) raindrop mixing ratio, and (f) precipitation rate for the 17 values of BANCs. Red lines signify the NEW cases, blue lines signify the MG08 cases, and black lines signify the TE14 cases.

3.2.3. Cold cloud simulations

For the second type of idealized simulations, a mixed-phase single-cell cloud is made with cloud base height of 1 km, maximum height of 10 km and width of 6 km. The cloud develops at 5 min and then dissipates at 50-60 min (Fig. 10). In the developing stage up to approximately 22 min, the cloud is mostly composed of liquid water. In the mature stage (22 to 35 min), ice hydrometeors are made and precipitation starts. The cloud properties such as CDNC, hydrometeor mixing ratios, cloud life time, and precipitation amount are affected by different parameterizations and BANCs, but the overall life cycle of the cloud remains similar in various cases.

In the developing stage (at 18 min), there is a strong updraft in the center of the cloud, accelerating as the air goes up inside the cloud with the maximum vertical velocity of 15 m s^{-1} at the cloud center (Fig 11a). Air converges into the cloud sides and base, rises up and diverges at the cloud top. Activation occurs mainly in two places, at the base of cloud center (2-km height) and at the cloud side (4-km height). The CDNC is highest at the base of the cloud center and has lower values in the upper clouds for all simulations (Fig 11). As the BANC increases, the CDNC increases, but the ratio of CDNC to BANC decreases, as in the warm cloud simulations. The MG08 cases show the largest CDNC, and the TE14 cases show the smallest CDNC within the same aerosol profiles. The TE14 and MG08 cases a similar

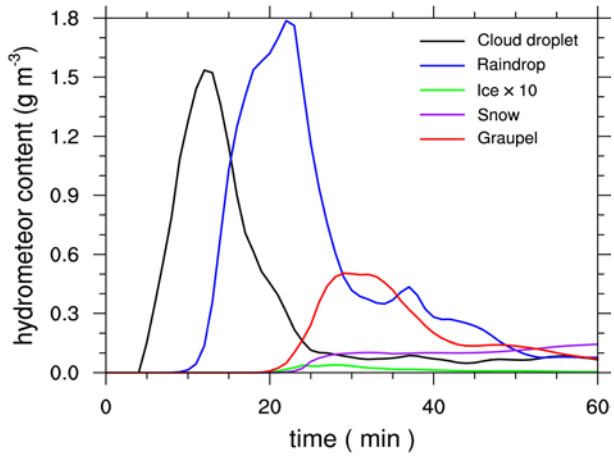

Figure 10. Time series of in-cloud averaged hydrometeor contents. Black, blue, green, purple, and red lines denote cloud droplets, raindrops, ice crystals multiplied by 10, snow, and graupel, respectively.

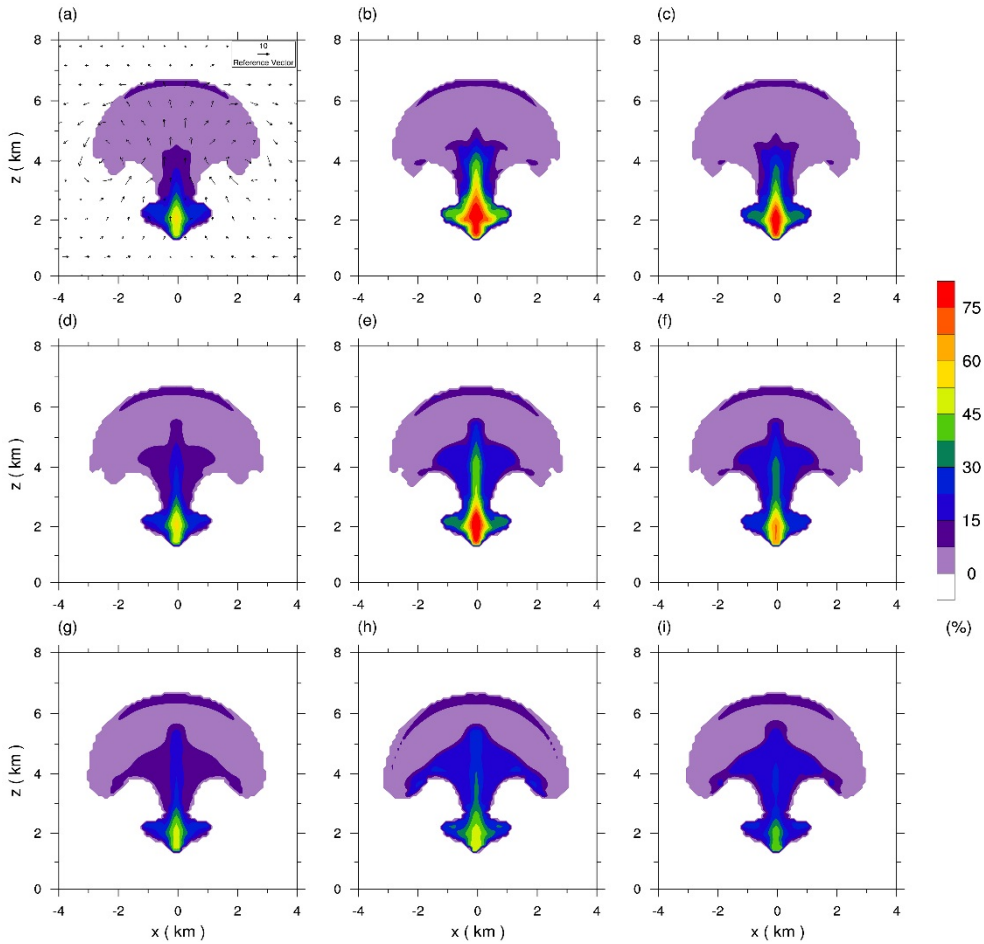

Figure 11. As in Fig. 6, but for the single-cell cloud simulations at 18 min. Black arrows in Fig. 11a represent wind vectors.

spatial pattern to that of the CDNC, with larger value in the MG08 cases, due to increased activation with increased potential aerosol number.

The in-cloud averaged CDNC in the NEW cases is in between those of the MG08 and TE14 cases, but its spatial distribution is quite different from the two simulations. In the NEW cases, the CDNC in the cloud center is much smaller than the MG08 cases and is even smaller than the TE14 cases for the polluted case. Meanwhile, the CDNC in the cloud side is similar to that of the MG08 cases and larger than that of the TE14 cases. In summary, the CDNC in the cloud center decreases and the CDNC in the cloud side increases compared with the spatial distribution of the MG08 and TE14 cases. This result indicates that activation in the cloud center is particularly suppressed by pre-existing cloud droplets and can be interpreted as follows. As in the orographic cloud simulations, the activation is reduced in the region where the vertical velocity increases as the air moves into the cloud. Cloud droplets formed at the very bottom of the cloud center increase their size as the air moves upward and inhibit the formation of new cloud droplets. In the cloud side, however, the highest vertical velocity appears when the air moves into the cloud, and the CDNC is determined at the cloud edge where no pre-existing cloud droplet exists, thus the CDNC values of the NEW cases are similar to those of the MG08 cases.

The CDNC changes initiated by activation also affect other microphysics processes, such as evaporation, conversion of cloud droplets into raindrops,

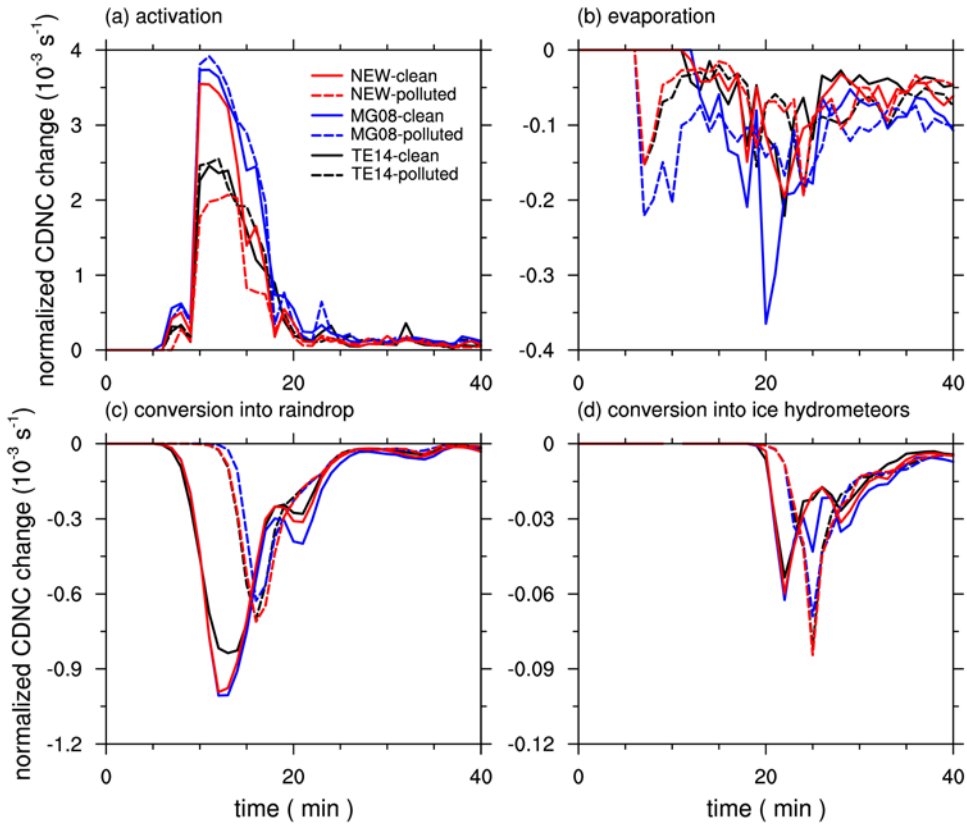

Figure 12. Time series of normalized CDNC change rate by (a) the activation, (b) the evaporation, (c) the conversion into raindrops, and (d) the conversion into ice hydrometeors. Red lines signify the NEW cases, blue lines signify the MG08 cases, and black lines signify the TE14 cases. Solid lines are the clean cases and dashed lines are the polluted cases.

and conversion of liquid hydrometeors into ice particles, snow, and graupel (Fig. 12). Activation prevails in the developing stage, when many cloud droplets are newly formed. Conversion into raindrops increases as the cloud develops, and conversion into ice hydrometeors subsequently occurs after the cloud droplets reach a freezing level. The normalized activation rate does not change much within the cases with the same parameterization in the MG08 and TE14 cases, but there is a substantial difference between the clean and polluted cases of the NEW cases (Fig. 12a). In the NEW cases, the clean case shows a larger normalized activation rate than the polluted case, in agreement with the orographic cloud simulations. This result implies that, for the deep cloud, the BANC significantly affects the activation fraction only in the NEW cases, when the maximum supersaturation decreases due to the pre-existing cloud droplets. Processes affecting the CDNC except activation do not depend much on the parameterization methods, but are more sensitive to the BANC. In the clean cases, raindrop formation is faster and larger (Fig. 12c) and evaporation occurs faster in the developing stage (Fig. 12b) than in the polluted cases, due to larger cloud droplet size. Ice hydrometeor formation is also faster in the clean cases but the amount is larger in the polluted cases (Fig. 12d).

For the MG08 and TE14 cases, the cloud droplet fractions are nearly constant, and the CDNC increases almost linearly as BANC increases (Figs. 13a and 13b). The differences between the MG08 and TE14 also remain at

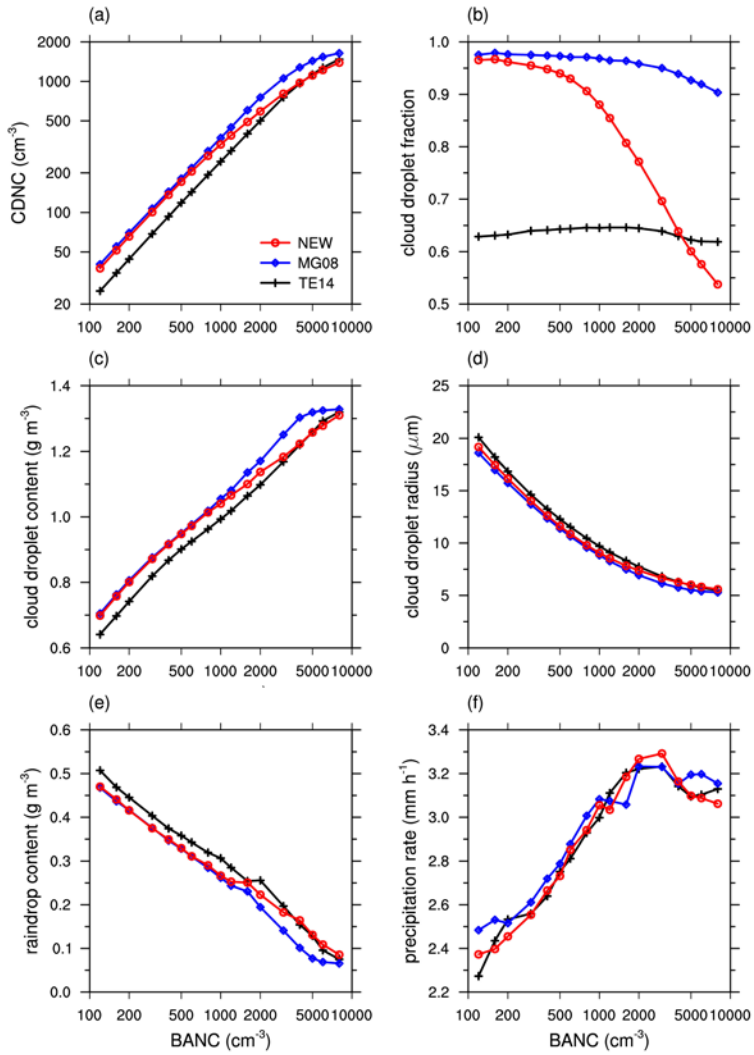

Figure 13. In-cloud averaged (a) CDNC and (b) cloud droplet fraction, domain-averaged (c) cloud droplet mixing ratio, (d) cloud droplet radius, and (e) raindrop mixing ratio averaged from 5 to 20 min (the developing stage), and (f) domain and 1-h averaged precipitation rate for the 17 values of BANCs.

large values (approximately two times in the CDNC and 0.35 in the cloud droplet fraction), indicating that within the entire range of the BANCs, the potential aerosol number differences results in a significant change in the activation fraction and the CDNC. Only the NEW cases show a decrease in the cloud droplet fraction in response to increasing BANC, especially in the polluted cases. This result shows that, in the deep cloud simulations, the effects of the pre-existing cloud droplets on supersaturation could be important only with sufficient aerosols. If the aerosols are limited, then the decrease in the maximum supersaturation by pre-existing cloud droplets does not affect the CDNC because there is a sufficient amount of excess vapor to condensate on the droplets and activate the aerosols. The cloud droplet mixing ratio increases by approximately two times with a 100 times increase of the BANC and is affected less than 20% by the choice of activation parameterizations (Fig. 13c). The effects of various BANCs and parameterizations on the cloud droplet content is negligible compared with the effects on the CDNC, thus, the droplet radius decreases 70% as the BANC increases, and the raindrop content averaged in the developing stage decreases in a manner similar to the orographic cloud cases (Figs. 13d and 13e). However, the total precipitation rate does not follow the trend of the raindrop mixing ratio in the developing stage; the total precipitation rate increases slightly (approximately 40%) up to the BANC of 4000 cm^{-3} and then decreases afterward (Fig. 13f). This result is consistent with the previous

study showing precipitation peaks between the aerosol number concentrations of 500 and 5000 cm^{-3} in idealized supercell thunderstorms with the moist soundings (Kalina et al. 2014).

3.2. Real case simulations

3.2.1. Experimental setup

To examine the effect of pre-existing cloud droplets in the real atmosphere, the New and MG08 parameterizations are compared through numerical simulations of a precipitation event in the Korean Peninsula. Weather Research and Forecast (WRF) model version 3.6 is also used for a real case study. As in the idealized simulations, the new and MG08 activation parameterizations are implemented in Thompson aerosol-aware microphysics scheme. Here, the TE14 method is not compared because the focus is only on the effect of pre-existing cloud droplets on superstation. For other physics parameterizations, RRTMG shortwave and longwave radiation scheme (Iacono et al. 2008), Yonsei University planetary boundary layer scheme (Hong et al. 2006) and Kain-Fritsch cumulus scheme (Kain 2004) for domains with grid spacing of 27 and 9 km are used.

The simulations were run for 42 h, starting at 12 UTC 22 July 2014. One day data from 06 UTC 23 to 06 UTC 24 July is used for the analysis, with a spin-up time of 18 hours. The model domain is composed of four nested domains with horizontal grid spacing of 27, 9, 3, and 1 km and time step of 81, 27, 9, and 3 s, respectively (Fig. 14). The vertical grids are 42 levels up to 50 hPa, with a vertical spacing of approximately 60 m near the surface.

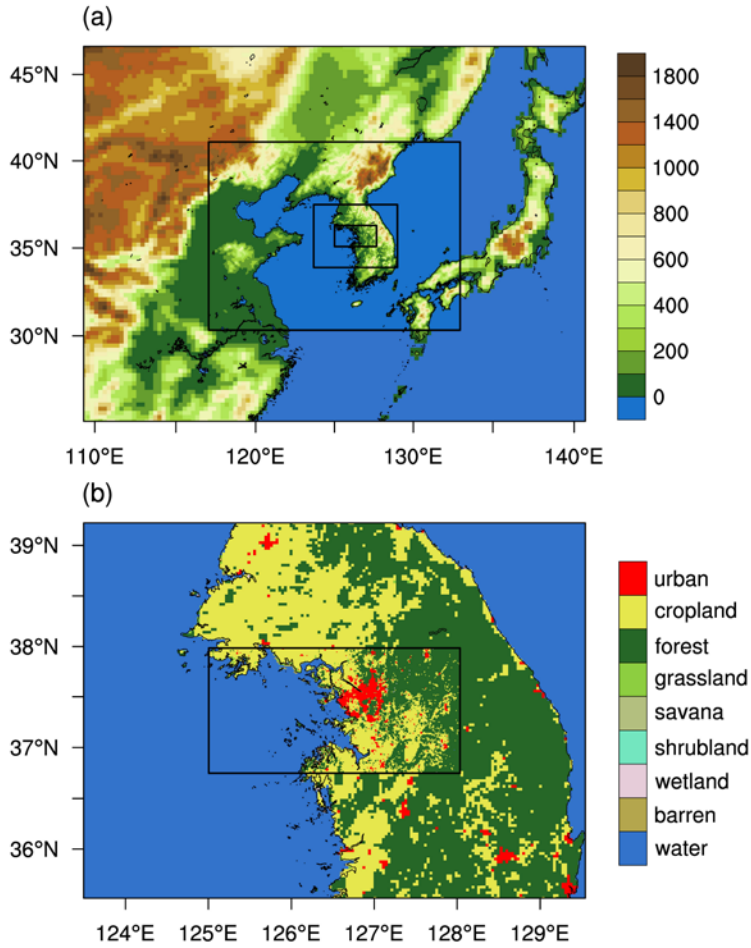

Figure 14. Model domain signifying (a) the topography (in m) for all 4 domains and (b) the land use types for the innermost 2 domains.

ERA-Interim reanalysis data with resolution of 0.7˚ is used for the initial and boundary data. The initial and boundary aerosol data are derived from multi-year (2001-2007) global model simulations (Colarco 2010), where the natural and anthropogenic sources by the Goddard Chemistry Aerosol Radiation and Transport (GOCART) model are regarded as emissions for particles and their precursors, as in Thompson and Eidhammer (2014).

According to the observation, from 06 UTC 23 to 06 UTC 24 July, the maximum 24-h accumulated precipitation was 67.5 mm and the maximum rainfall rate was 20 mm/hr near Seoul Metropolitan area. The precipitation system exists across the Korean peninsula, and frequent precipitation events occurred before and after the selected event. The synoptic pattern from the simulation near the onset of the precipitation event (12 UTC 23 July, 24 h after the simulation starts) is compared with the weather chart from the Korea Meteorological Administration (Fig. 15). The surface pressure chart shows a typical summer surface pressure pattern with high pressure system in the south-east and north-west of the Korean peninsula. A surface convergence is observed in the Yellow sea with southerly in the south and northerly in the north. At 850 hPa, the simulated geopotential and temperature pattern is quite similar to the observation and the moisture flux comes from the south-east China, which conveys sufficient moisture to the Korean peninsula with the westerlies. An upcoming typhoon is observed near the south China, but it does not affect the precipitation event directly until the simulation ends.

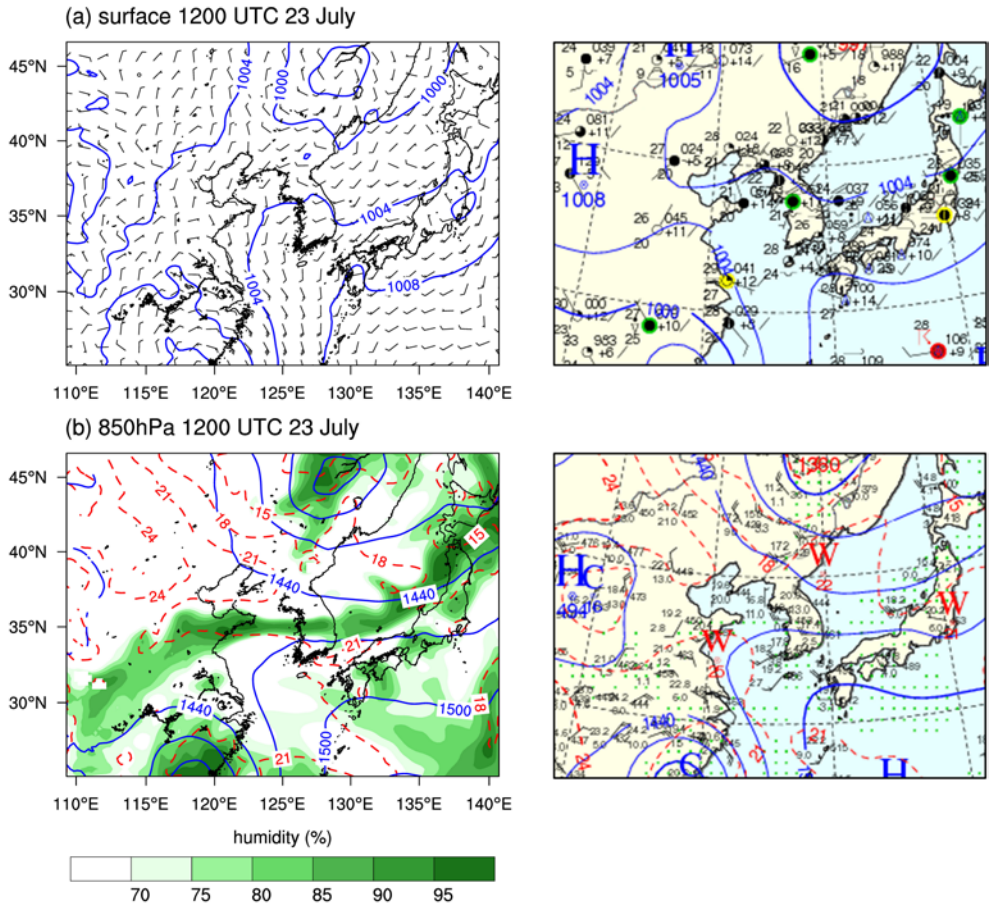

Figure 15. Synoptic charts at 12 UTC 23 July (24 h after the simulation starts). (a) Surface chart with the surface pressure (blue lines, in hPa) and 2-m wind vector (black arrows), and (b) 850-hPa chart with the geopotential height (blue solid lines, in m), the temperature (red dashed lines, in °C), and the humidity (green contours). The left column is the simulation result of the NEW case and the right column is from KMA.

3.2.2. Results

12 hour-accumulated precipitation patterns (from 15 UTC 23 to 03 UTC 24 July) of the innermost domain are compared with the AWS data (Fig. 16). The simulations underestimate the width of the precipitation band, but the maximum precipitation amount and the location of the band is well predicted. Although the difference between the simulations is small compared with the differences between the simulation results and observation, the NEW case shows more precipitation in the west of Seoul and less precipitation in the downwind side of the Seoul area compared with the MG08 case.

The temporal evolutions of the domain-averaged precipitation show that the precipitation event mainly occurs at night time (from 03 to 09 LTC 24 July) and there is a small amount of stratiform precipitation before the event (Fig. 17). Compared with the MG08 case, the NEW case shows a smaller amount of accumulated and hourly precipitation. Here, the cloud top is defined as the highest level with a cloud droplet content greater than 0.01 g/m^3, and a deep cloud is configured as a grid point with the cloud top higher than 4 km (near the freezing level). Using this definition, the differences of precipitation are significant under the deep clouds and almost the same as that of the total precipitation. This result indicates that deep clouds are responsible for a small amount of the total precipitation, but the precipitation differences between the simulations are largely caused by convective precipitation.

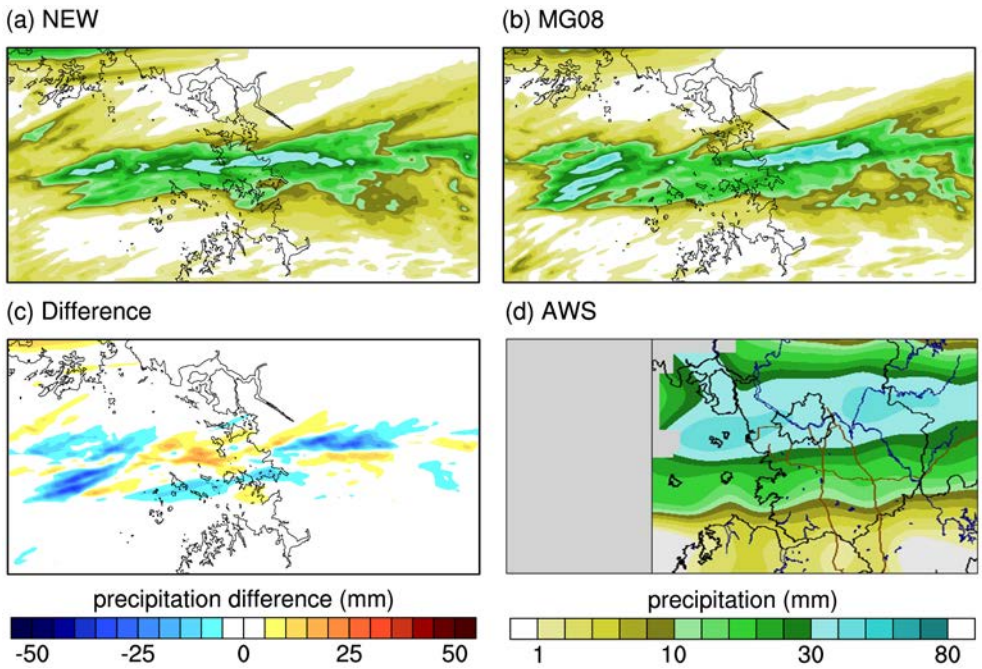

Figure 16. 12-h accumulated precipitation (from 15 UTC 23 to 03 UTC 24 July) of (a) the NEW case, (b) the MG08 case, (c) the difference between the NEW and MG08 cases, and (d) the observation data from AWS.

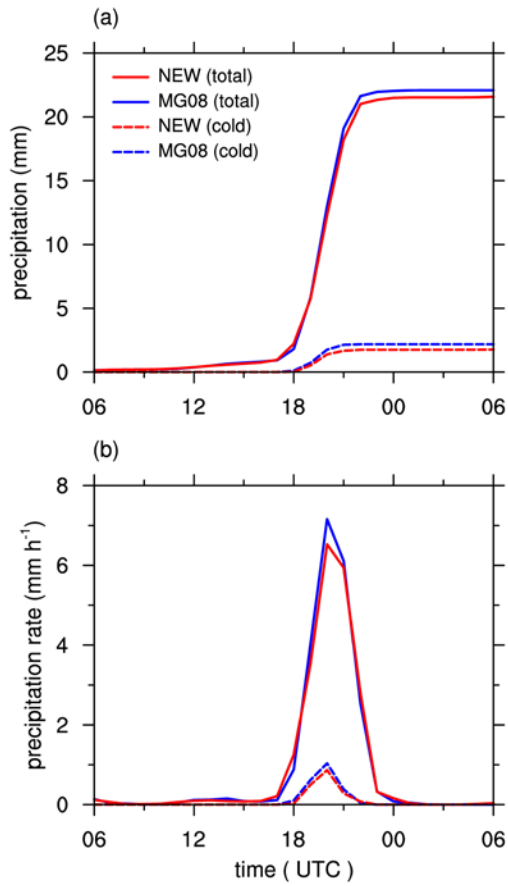

Figure 17. Time series of domain-averaged (a) accumulated precipitation and (b) precipitation rate in the innermost domain. Blue lines signify the MG08 case and red lines signify the NEW case.

The simulation results regarding the precipitation system development are generally similar between the NEW and MG08 cases, and the cloud formation as well as the precipitation exhibit similar patterns in time (Figs. 17 and 18). The in-cloud averaged CDNC is lower in the NEW case than in the MG08 case, with the smallest number when the deep clouds are developed (Fig. 18a). Because the CDNC in the upper clouds is small compared with the CDNC in the warm levels (Fig. 20b), the averaged CDNC must be smaller if the deep clouds dominate. Additionally, the CDNC differences between the cases are smallest at that period, because the cloud droplet fraction varies between the cases only in the lower warm clouds. The cloud droplet content does not differ substantially between the parameterizations, but the tendency is quite concrete (Fig. 18b). The NEW cases shows lower cloud droplet contents. The raindrop content shows a similar trend as that of the cloud droplet content (Fig. 18c), except there is almost no rain in the warm cloud dominating period. Note that a decrease in CDNC could delay and reduce freezing of cloud droplets in the idealized deep cloud simulation. Ice hydrometeor formation occurs only when deep clouds are developed (Fig. 18d), and it starts later and in a smaller amount in the NEW case. The differences of the ice hydrometeor contents between the cases are greater than the differences of the cloud droplet and raindrop contents, i.e., suppression in the formation of ice hydrometeors is more significant than that of liquid hydrometeors in the NEW case.

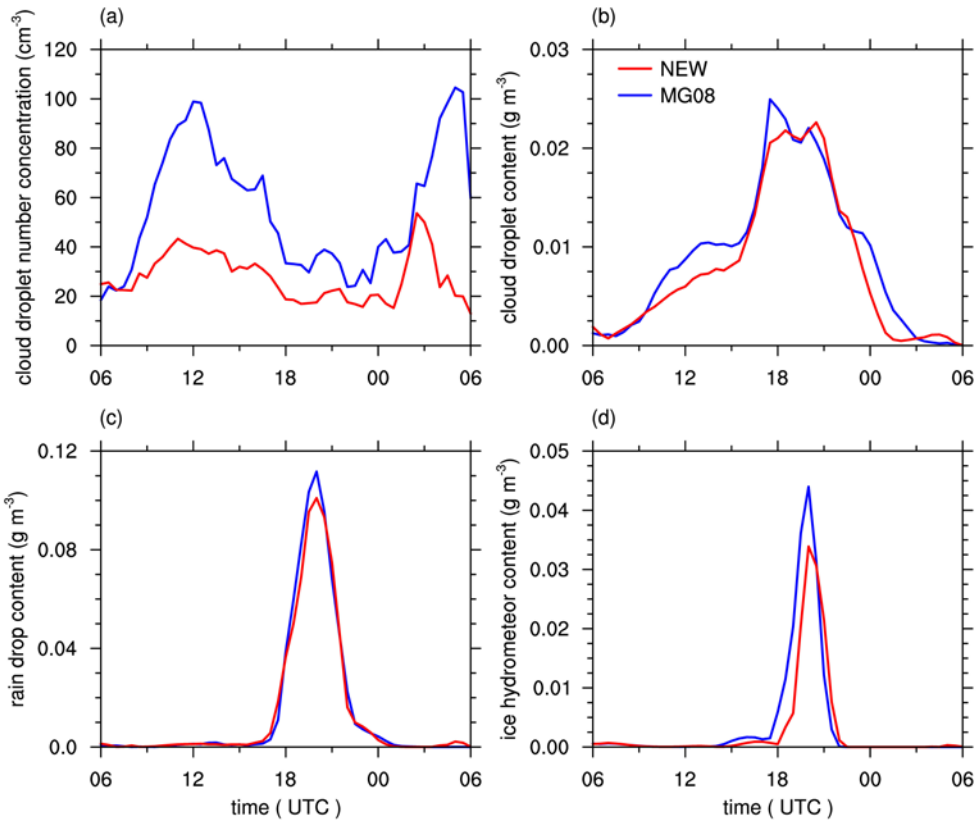

Figure 18. Time series during the 24-h analysis time of (a) in-cloud averaged CDNC, domain-averaged (b) clod droplet contents, (c) raindrop contents, and (d) ice hydrometeor contents. Blue lines signify the MG08 case and red lines signify the NEW case.

As seen in the vertical cross-sections of hydrometeor mixing ratios (Figs. 19a and 19c), warm clouds cover almost all the area across the west of Korean Peninsula below the height of 3 km, with deep clouds of smaller horizontal scale up to 14 km in height. Warm clouds are continuously formed in the lower atmosphere and induces a light precipitation. Deep convective clouds are generated at 15 UTC 23, and then move to the east, resulting in intense precipitation. The cloud droplet fraction is almost 100% in the clouds above the height of 4 km in both simulations, whereas the cloud droplet fraction in the lower levels is lower in the NEW case (Figs. 19b and 19d). In these cases, the aerosol concentration above 2 km is quite small (Fig. 20d) and the deep clouds usually have a stronger updraft than the warm clouds, so that the cloud droplet fraction is always near 100% in the upper levels, regardless of the activation parameterizations. In the lower levels, which have higher aerosol concentration, the effect of pre-existing cloud droplets can be significant enough to reduce the CDNC and cloud droplet fraction in the NEW case.

The microphysical properties of the clouds can also be deduced from the vertical profiles (Fig. 20). The aerosol number concentration decreases rapidly as the height increases, and it becomes quite small above 2 km. In the lower levels, there comparatively are more aerosols in NEW case due to the lower CDNC and precipitation amount. In-cloud averaged CDNC is highest at near the height of 1 km up to 90 and 40 cm^{-3} in the MG08 and NEW cases, respectively. In contrast, the CDNC is always less than 10 cm^{-3} in the upper

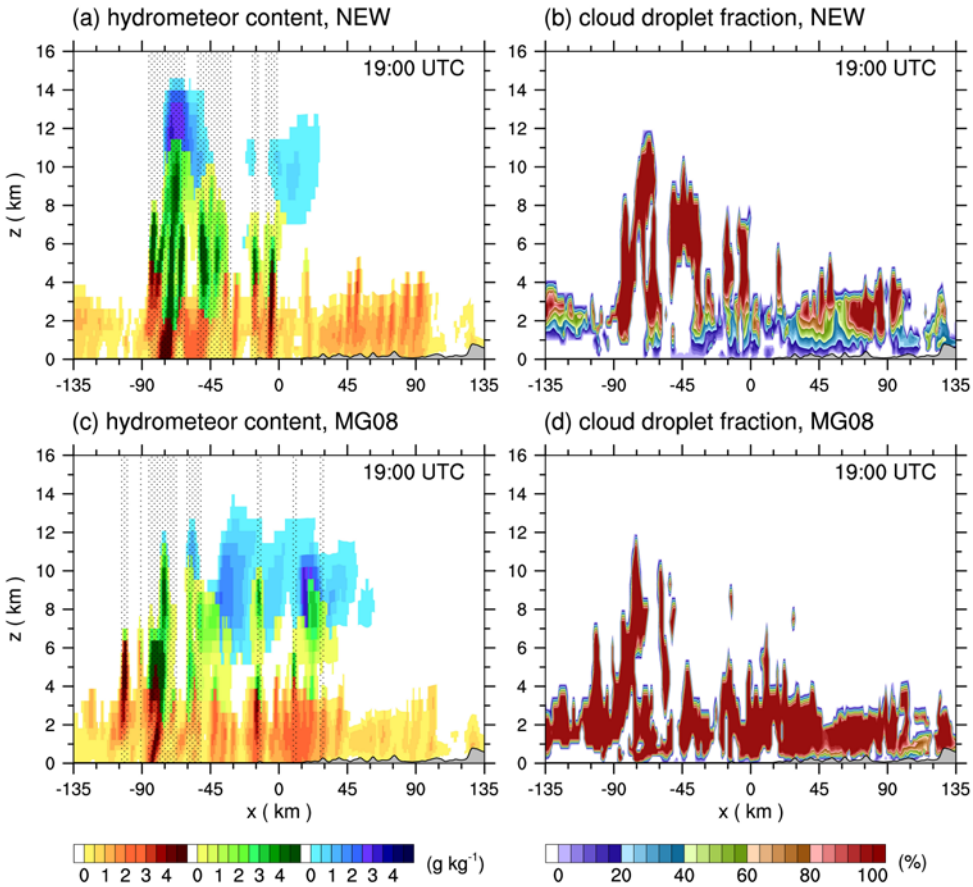

Figure 19. XZ cross-section of (a) the hydrometeor content of the NEW case, (b) the cloud droplet fraction of the NEW case, (c) the hydrometeor content of the MG08 case, and (d) the cloud droplet fraction of the MG08 case. Red, green, and blue contours in (a) and (c) signify the liquid water mixing ratio, liquid and ice water mixing ratio, and ice water mixing ratio, respectively. Dotted area is considered as deep cloud, where cloud top is above the freezing level.

levels, because there are a small number of aerosols. The liquid water content is lower in the NEW case, especially in the lower levels, where the CDNC is lower than that of the MG08 case. The lower liquid water content in the warm cloud level and the similar amount of precipitation from the warm cloud, shows that the NEW case has higher efficiency to form rainfall, due to the increased droplet size. Ice water reduction is clearly shown in the NEW case, and the differences between the cases of ice water reduction are larger than the differences in the liquid water reduction. This result indicates that there must be another mechanism that affects the precipitation system to inhibit the cold cloud formation rather than the reduced formation of liquid water.

The reduction in the liquid hydrometeor contents is further analyzed under the division of warm and cold (deep) clouds (Fig. 21). The dominant cloud level is very low (under 2 km) for the warm clouds and it is approximately 4-5 km (near the freezing level) for the cold clouds. This division reveals that the suppression of both cloud droplets and raindrops with the new parameterization is dominant in the warm clouds. The relative strength of reduction is lower for the raindrops, indicating that the efficiency of the conversion of cloud droplets into raindrops is higher in the NEW case. In the cold clouds, there is a slight enhancement of cloud droplet and raindrop mixing ratio above the height of 2 km. This result can be interpreted as having more cloud droplets remaining in liquid form because of the reduced freezing and collisions with the lower amount of ice hydrometeors.

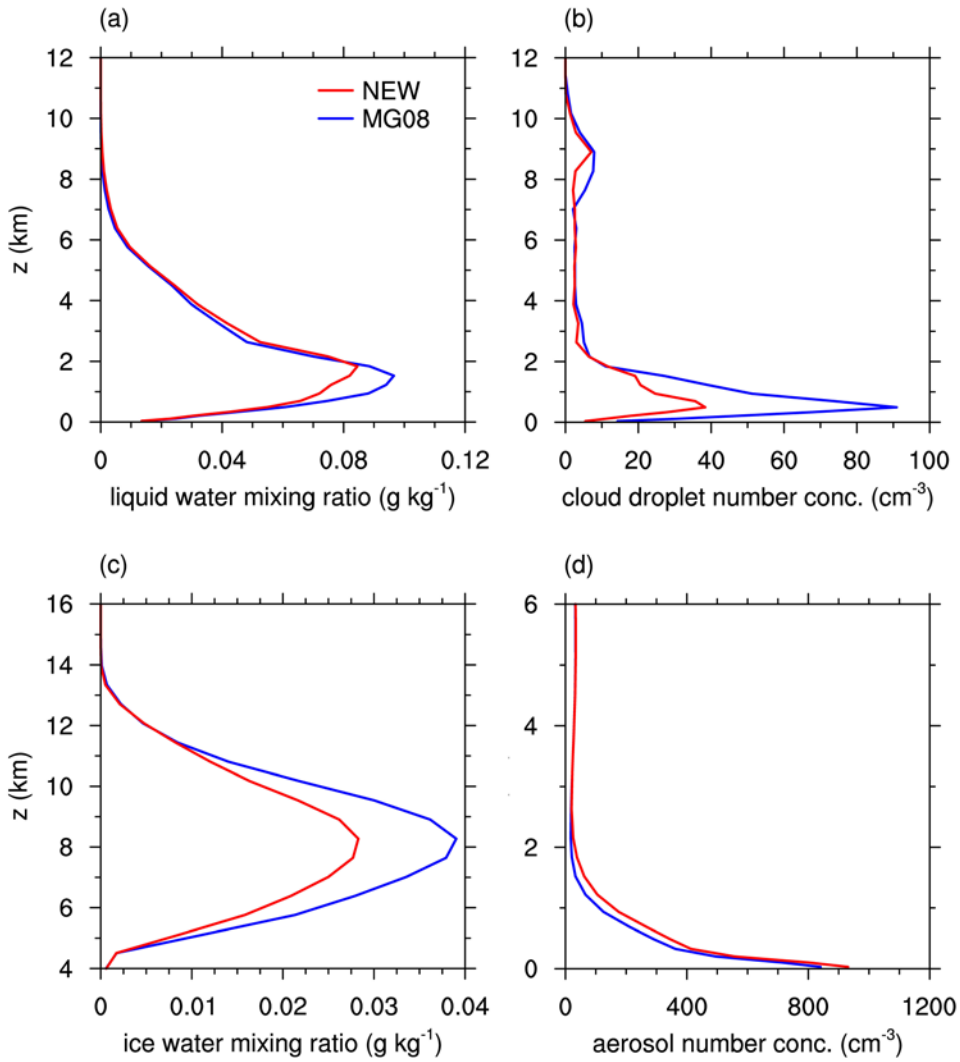

Figure 20. Vertical profiles of (a) domain-averaged liquid water mixing ratio, (b) in-cloud averaged CDNC, (c) domain-averaged ice water mixing ratio, and (d) domain-averaged aerosol number concentration. Blue lines signify the MG08 case and red lines signify the NEW case.

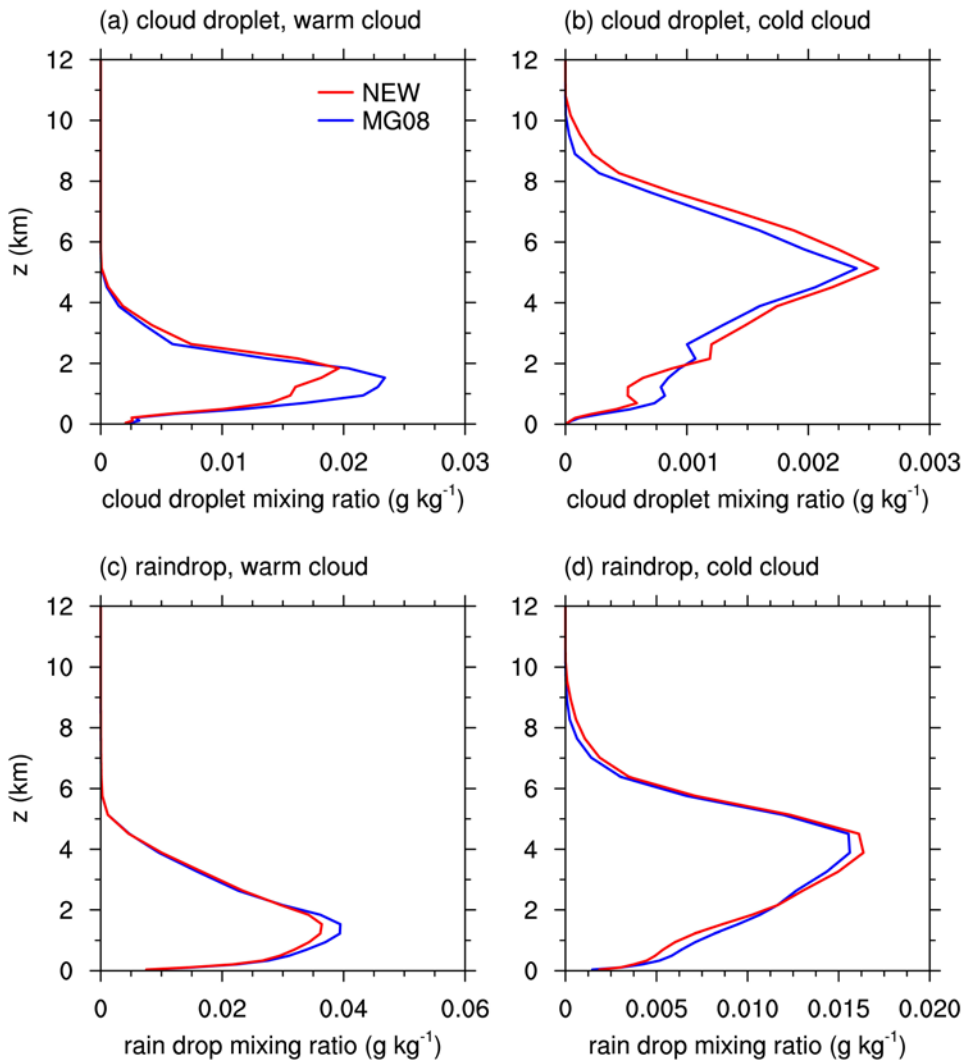

Figure 21. Vertical profiles of domain-averaged (a) cloud droplet mixing ratio from warm clouds, (b) cloud droplet mixing ratio from cold clouds, (c) raindrop mixing ratio from warm clouds, and (d) raindrop mixing ratio from cold clouds.

The differences in the cloud droplet and raindrop mixing ratio between the NEW and MG08 cases can be explained by the condensation and the warm rain conversion rate, which are the most important processes regarding warm cloud microphysics (Figs. 22a and 22b). The total amount of condensation is similar in both cases because it is determined mostly by the environmental variables. However, despite the smaller amount of cloud droplets, warm rain conversion is enhanced lightly in the NEW case. This result is consistent with the hypothesis discussed earlier, i.e., increased size of cloud droplets due to the smaller CDNC increases the efficiency of warm rain formation, resulting a smaller reduction in the raindrop mixing ratio compared with that of cloud droplet mixing ratio.

Regarding the growth of ice hydrometeors, the freezing and deposition occur in a smaller amount in the NEW case compared with the MG08 case, thereby decreasing the amount of ice hydrometeors and suppressing the formation of deep clouds (Figs. 22c and 22d). The decrease in formation of ice hydrometeor can be considered in the same manner as the idealized deep cloud simulation. The small CDNC results in large cloud droplets and prohibits the droplets to rise above the height of 9 km, where cloud droplets and raindrops can freeze into ice hydrometeors. With decreased number and amount of ice crystals, the deposition rate must decrease as well. There is also a decrease in collisions between the ice and liquid hydrometeors as less ice hydrometeors fall into the mixed cloud layer (not shown), resulting in

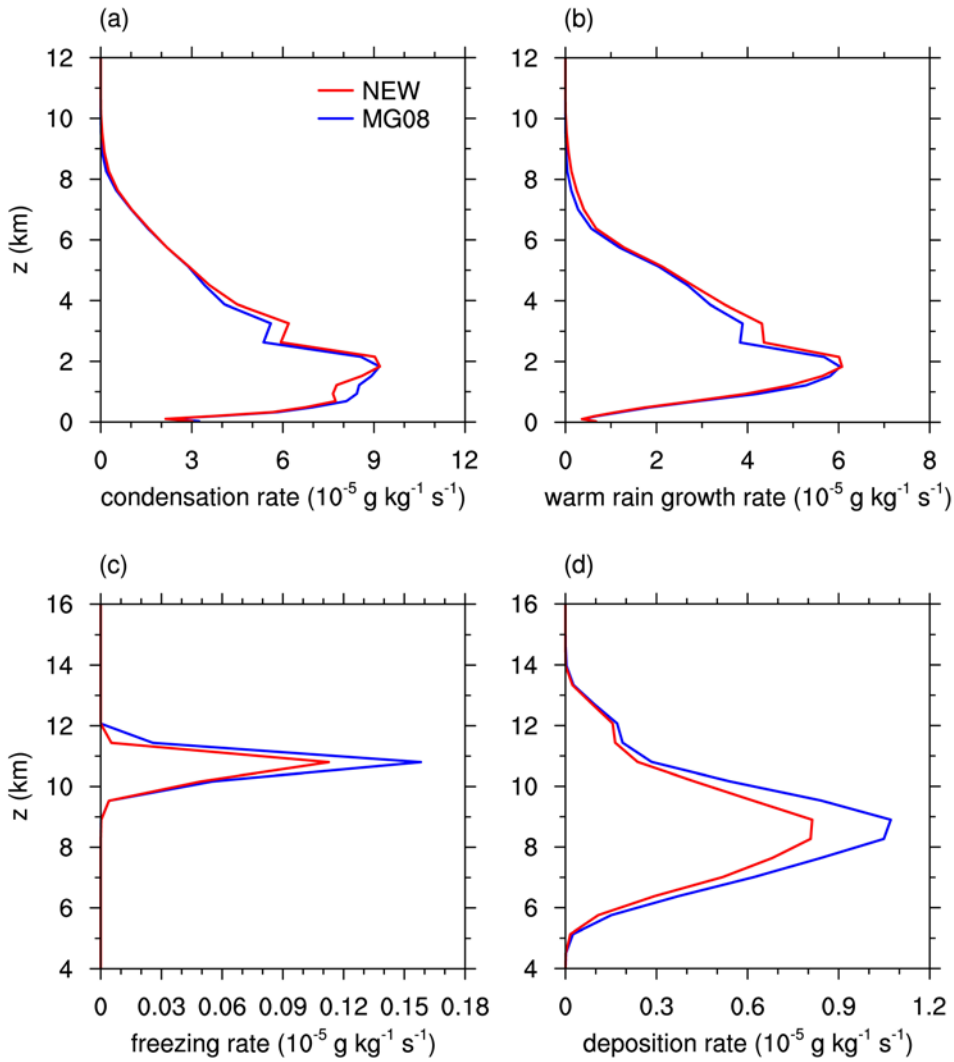

Figure 22. Vertical profiles of domain-averaged process rates. (a) Condensation onto cloud droplets, (b) conversion of cloud droplets into raindrops, (c) freezing of cloud droplets and raindrops into ice crystals, and (d) deposition onto ice crystals and snow.

larger amount of liquid water remaining near the height of 4-6 km (Fig. 21c and 21d).

The aerosol and cloud droplet number concentrations of the simulations with the climatological aerosol inputs are compared with the two simulations performed using the BANC of 500 cm^{-3} (clean) and 5000 cm^{-3} (polluted) (Fig. 23). Because of the precipitation event before the analysis period, the aerosol number concentration decreases for the first 3 h, and then recovers slightly before the formation of deep clouds and precipitation. After 18 UTC 23, the aerosol number concentration decreases by 1/4 times, because of the wet scavenging process accompanied with precipitation and increased activation process. Both the aerosol number concentration and the CDNC from climatological data are in between the results of the clean and polluted cases. The polluted case shows an aerosol number concentration more than 15 times than that of the clean case, but the CDNC difference is less than 10 times. The sensitivity of the CDNC change between the two parameterizations appears to increase in the polluted case, but their detailed behaviors are not analyzed here.

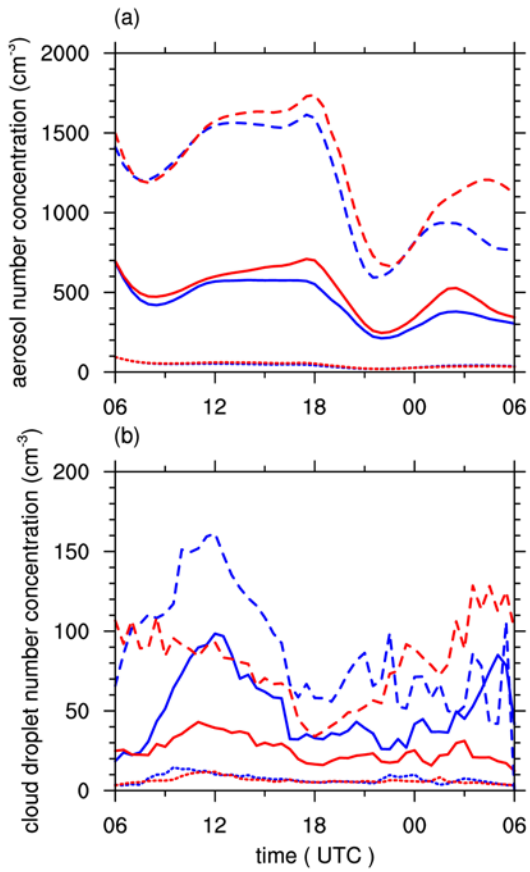

Figure 23. Time series of (a) aerosol number concentration averaged in the lowest 2-km level and (b) in-cloud averaged CDNC. Blue lines signify the MG08 cases and red lines signify the NEW cases. Solid lines refer to the simulations with the climatological data, small dashed lines refer to the control cases, and long dashed lines refer to the polluted cases.

4. Summary and conclusions

To extend the validity of an activation parameterization to the in-cloud environment, the effects of pre-existing cloud droplets were investigated in two ways. Pre-existing cloud droplets are regarded as previously activated aerosols and increase the number of potential aerosols, increasing the calculated value of the CDNC. Meanwhile, as the consumer of supersaturation, they prohibit the activation process by depleting excess vapor in advance of the aerosols. By adding the growth rate of the pre-existing cloud droplets to the activation parameterization, the activation fraction decreases with increasing cloud droplet size and population. The suppression is significant in the environment with low vertical velocity and high aerosol concentration.

In the idealized cloud simulations, the CDNC decreases by considering pre-existing cloud droplets on calculation of the maximum supersaturation, especially in the region that is favorable for in-cloud activation. The middle region of the orographic cloud and the center of the single-cell cloud are the places where the vertical velocity increases as the air parcel moves into the cloud. It is studied using the bin microphysics scheme by Pinsky and Khain (2002) that even with the same maximum vertical velocity at the cloud center, the low updraft velocity at the cloud base results in a smaller CDNC, because in-cloud activation does not produce new cloud droplets as much as in the

environment without cloud droplets. The new parameterization enables representation of this feature, by reducing the CDNC in the regions with higher vertical velocity at the cloud center compared with the cloud base.

The effect of pre-existing cloud droplets on supersaturation (differences between the NEW and MG08 cases) is more crucial to the activation fraction than the effect of droplets on the potential aerosol number (differences between the MG08 and TE14 cases) in the orographic cloud simulations, and vice versa in the single-cell cloud simulations. These different trends can be explained by the different regimes of cloud droplet formation introduced in Reutter et al. (2009). The orographic cloud case is classified as the updraft-limited regime, having a sufficient amount of aerosols compared with the supply of supersaturation, whereas the single-cell cloud case is categorized as the aerosol-limited regime, having adequate supersaturation compared with the aerosol supply. In updraft-limited regimes, changes in the BANC do not affect the CDNC as much as those in aerosol-limited regimes. Because the aerosol number concentration is not a primary factor determining the activation rate in the orographic cloud case, the pre-existing cloud droplets affect activation more significantly through competition for supersaturation. In contrast, in the single-cell cloud case where the activation rate is substantially affected by the aerosol number concentration, changes in the potential aerosol number are more important than the changes in supersaturation due to pre-existing droplets.

In addition to the two idealized simulations, the new parameterization was implemented for a real precipitation system composed of wide, shallow and continuous warm clouds and deep clouds passing through the Korean Peninsula with intense precipitation. It is clearly seen that the new parameterization decreases the cloud droplet number concentration and suppresses the formation of deep clouds, whereas warm cloud processes to form raindrops are more efficient with the new parameterization, as in the idealized cold cloud simulations.

The goal of this study is to parameterize in-cloud activation using cloud droplet radius and number concentration. To represent the in-cloud environment, the new parameterization uses two more prognostic variables, which are already given in two-moment bulk microphysics schemes. The parameterization could be easily adapted in other two-moment microphysics schemes to avoid overestimation of the in-cloud activation caused by ignoring the effects of pre-existing cloud droplets on supersaturation. To validate the parameterization further, a statistical approach of various types of real case simulations or long-term tests is required. Development of the parameterization with a realistic size distribution of pre-existing cloud droplets such as gamma distributions, could also be attempted.

References

Abdul-Razzak, H., S. J. Ghan, and C. Rivera-Carpio, 1998: A parameterization of aerosol activation 1. Single aerosol type. *J. Geophys. Res.*, **103**, 6123-6131.

_____, and S. J. Ghan, 2002: A parameterization of aerosol activation 3. Sectional representation. *J. Geophys. Res.*, **107(D3)**, 4026, doi:10.1029/2001JD000483.

Albrecht, B., 1989: Aerosols, cloud microphysics, and fractional cloudiness. *Science*, **245**, 1227–1230.

Barahona, D., R. E. L. West, P. Stier, S. Romakkaniemi, H. Kokkola, and A. Nenes, 2010: Comprehensively accounting for the effect of giant CCN in cloud activation parameterizations. *Atmos. Chem. Phys*., **10**, 2467-2473.

Eidhammer, T., P. J. DeMott, and S. M. Kreidenweis, 2009: A comparison of heterogeneous ice nucleation parameterizations using a parcel model framework. *J. Geophys. Res*., **114**, D06202, doi:10.1029/2008JD011095.

Feingold, G., and A. J. Heymsfield, 1992: Parameterizations of condensational growth of droplets for use in general circulation models. *J. Atmos. Sci*., **49**, 2325–2342

Flossman, A. I., W. D. Hall, and H. R. Pruppacher, 1985: A theoretical study

of the wet removal of atmospheric pollutants. Part I: The redistribution of aerosol particles captured through nucleation and impaction scavenging by growing cloud drops. *J. Atmos. Sci*., **42**, 582–606.

Fountoukis, C., and A. Nenes, 2005: Continued development of a cloud droplet formation parameterization for global climate models. *J. Geophys. Res.*, **110**, D11212, doi:10.1029/2004JD005591.

Ghan, S. J., H. Abdul-Razzak, A. Nenes, Y. Ming, X. Liu, M. Ovchinnihov, B. Shipway, N. Meskhidze, J. Xu, and X. Shi, 2011: Droplet nucleation: Physically-based parameterizations and comparative evaluation. *J. Adv. Model. Earth Syst.*, **3**, M10001, doi:10.1029/2011MS000074.

Grell, G. A., S.E. Peckham, R. Schmitz, S. A. McKeen, G. Frost, W. C. Shamarock, and B. Eder, 2005: Fully coupled “online” chemistry within the WRF model. *Atmos. Environ.*, **39**, 6957-6975.

Hong, S. Y., Y. Noh, and J. Dudhia, 2006: A new vertical diffusion package with an explicit treatment of entrainment processes, *Mon. Wea. Rev.*, **134**, 2318-2341.

Iacono, M. J., J. S. Delamere, E. J. Mlawer, M.W. Shephard, S. A. Clough, and W. D. Collins, 2008: Radiative forcing by long-lived greenhouse gases: calculations with the AER radiative transfer models, *J. Geophy. Res*., **113**, D13103, doi:10.1029/2008JD009944.

Janjic, J. I, 1994: The step-mountain eta coordinate model: further developments of the convection, viscous sublayer, and turbulence closure schemes, *Mon. Wea. Rev*. **122**, 927-945.

Kain, J. S., 2004: The Kain-Fritsch convection parameterization: an update, *J. Appl. Meteor.*, **43**, 170-181

Khain, A. P., L. R. Leung, B. Lynn, and S. Ghan, 2009: Effects of aerosols on the dynamics and microphysics of squall lines simulated by spectral bin and bulk parameterization schemes. *J. Geophys. Res*., **114**, D22203, doi:10.1029/2009JD011902.

Lebo, Z. J., and J. H. Seinfeld, 2011: A continuous spectral aerosol-droplet microphysics model. *Atmos. Chem. Phys*., **11**, 12297–12316.

_____, and H. Morrison, 2013: A novel scheme for parameterizing aerosol processing in warm clouds. *J. Atmos. Sci.*, **70**, 3576-3598.

_____, and H. Morrison, 2014: Dynamical effects of aerosol perturbations on simulated idealized squall lines. *Mon. Wea. Rev.*, **142**, 991-1009.

Lim, K. S., and S. Y. Hong, 2009: Development of an effective double-moment cloud microphysics scheme with prognostic cloud condensation nuclei (CCN) for weather and climate models. *Mon. Wea. Rev.*, **138**, 1587-1612.

Ming, Y., V. Ramaswamy, L. J. Donner, and V. T. J. Phillips, 2006: A new parameterization of cloud droplet activation applicable to general circulation models. *J. Atmos. Sci.*, **63**, 1348-1356.

Nenes, A., S. Ghan, H. Abdul-Razzak, P. Y. Chuang, and J. H. Seinfeld, 2001, Kinetic limitations on cloud droplet formation and impact on cloud albedo, *Tellus*, Ser. B, **53**, 133–149.

_____, and J. H. Seinfeld, 2003: Parameterization of cloud droplet formation in global climate models. *J. Geophys. Res*., **108 (D14)**, 4415, doi:10.1029/2002JD00291.

Pinsky, M. B., and A. P. Khain, 2002: Effects of in-cloud nucleation and turbulence on droplet spectrum formation in cumulus clouds. *Q. J. R. Meteorol. Soc.*, **128**, 501-533.

Pruppacher, H. R., and J. D. Klett, 1997: *Microphysics of Clouds and Precipitation*. Kluwer, 954 pp.

Reutter, P., H. Su, J. Trentmann, M. Simmel, D. Rose, S. S. Gunthe, H. Wernli, M. O. Andreae, and U. Pöschl, 2009: Aerosol- and updraft-limited regimes of cloud droplet formation: influence of particle number, size, and hygroscopicity on the activation of cloud condensation nuclei (CCN). *Atmos. Chem. Phys*., **9**, 7067–7080.

Thompson, G., and T. Eidhammer, 2014: A study of aerosol impacts on clouds and precipitation development in a large winter cyclone. *J. Atmos. Sci.*, **71**, 3636-3658.

Twomey, S., 1974: Pollution and the planetary albedo. *Atmos. Environ.*, **8**, 1251–1256.

_____, 1977: Influence of pollution on shortwave albedo of clouds, *J. Atmos.*

Sci., **34**, 1149–1152.

초록

상승하는 단열 공기 덩이에 대한 구름 응결핵 활성화 과정을 온도, 연직 속도, 에어로졸과 구름 방울의 수농도, 구름 방울 반지름을 이용하여 모수화한다. 새로운 모수화 방법은 기존에 존재하는 구름 방울이 공기 덩이의 최대 과포화도에 미치는 영향을 포함하여 구름 내부에서의 활성화 과정을 고려한다. 구름 방울 내의 구름 응결핵을 잠재 에어로졸 수에 포함시켜 에어로졸 수농도와 크기 분포 또한 개선하였다. 새로운 모수화 방법은 WRF 모형의 Thompson aerosol-aware 미시 물리 과정에 적용되었다. 잠재 에어로졸이 증가하면서 구름 방울 개수는 증가하고, 기존 구름 방울로 인해 최대 과포화도가 줄어들면서 구름 가장자리에 비해 구름 내부에서 활성화 과정이 감소하였다. 결과적으로, 이전의 모수화를 사용한 경우 연직 속도가 가장 큰 곳에서 구름 방울 수농도가 가장 높지만, 새로운 모수화를 사용한 경우 구름이 생성되는 부분 근처에서 구름 방울 수농도가 가장 높다. 에어로졸 수농도의 증가보다 기존 구름 방울로 인한 과포화도 감소가 더 중요한 상승 속도 제한 영역에서 새로운 모수화 방법은 구름 방울 수농도를 감소시킨다. 반대로 에어로졸 제한 영역에서는 에어로졸

수농도 증가가 활성화 과정에 더 많은 영향을 미쳐 구름 방울 수농도가 감소한다. 이상적인 온난 구름 모의 (상승 속도 제한 영역) 결과, 감소한 구름 방울 수농도는 구름 방울의 크기를 증가시키고 더 많은 강수를 유발한다. 이상적인 깊은 대류 구름 모의 (에어로졸 제한 영역) 결과, 증가한 구름 방울 수농도는 발달 단계에서의 빗방울 형성을 감소시키지만, 성숙 단계에서는 더 많은 구름 방울이 결빙 고도 위로 상승해 잠열을 방출하고 연직 운동을 강화시킨다. 새로운 모수화 방법과 에어로졸 기후 자료를 이용해 지속적으로 온난 구름이 생성되면서 깊은 대류가 강한 강수를 유발하는 2014년 7월 24일 한반도 강수 사례를 수치 모의하였다. 새로운 모수화 방법을 사용한 경우 이상적인 수치 모의에서와 같이 구름 방울의 수농도가 감소하였고, 온난 구름에서는 빗방울 형성이 증가하는 반면 깊은 대류 구름에서는 얼음 대기 수상과 강수량이 감소하였다.

주요어 : 구름 응결핵 활성화, 구름 내부에서의 핵형성, 미세 물리 과정 모수화, 구름 방울 수농도, 이중 모멘트 구름 미세 물리
학번 : 2013-22968